Bonding in Low-Coordinate Complexes

What, if anything, is special?

Espen Tangen

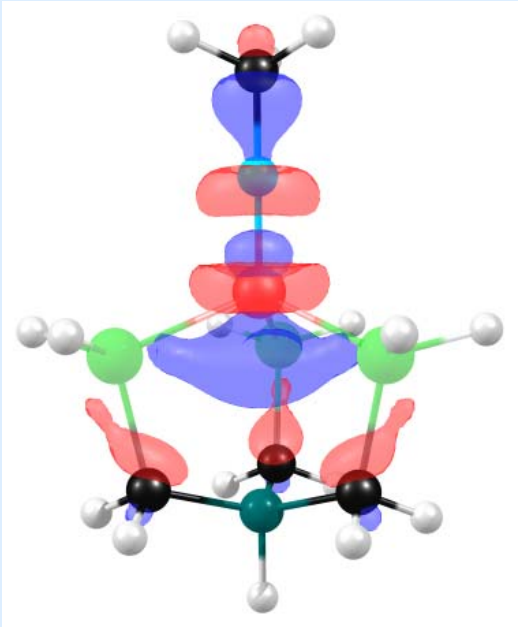

A dissertation for the degree of Philosophiae Doctor

UNIVERSITY OF TROMSØ
Faculty of Science
Centre for Theoretical and Computational Chemistry
Department of Chemistry

September 2008

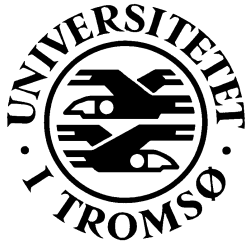

A DISSERTATION FOR THE DEGREE OF PHILOSOPHIAE DOCTOR

BONDING IN LOW-COORDINATE COMPLEXES

WHAT, IF ANYTHING, IS SPECIAL?

Espen Tangen

September 2008

Centre for Theoretical and Computational Chemistry
Department of Chemistry, Faculty of Science
University of Tromsø, N-9037 Tromsø, Norway

ABSTRACT

To contribute to the fundamental picture of the electronic structure of low-coordinate transition metal complexes, we have carried out a series of DFT studies on mono-imido and nitrosyl complexes for different metal ions ($Mn^{II/III}$, $Fe^{II/III/IV}$, $Co^{II/III}$) and different systems of basal ligands. These studies reveal striking similarities of the electronic structure for these systems. The distinction of bent versus linear NO units is attributed to the ranking of the d_{z^2} and $d_{xz/yz}$ parentage MOs relative to each other. Without a ligand trans to the NO group, the antibonding metal d_{z^2}- NO σ orbital interaction is lessened by mixing in metal p_z, causing the MO to shift away from the NO ligand. This exact same orbital interaction appears to explain the existence of middle to late first-row transition metal imido complexes.

Keywords: Transition metals, DFT, low-coordinate, imido, nitrosyl, molecular orbitals.

Front cover: The metal d_{z^2} - imido σ orbital antibonding combination of a simple Fe^{IV}-imido model.

ACKNOWLEDGEMENTS

The work leading to this thesis was carried out at the Chemistry Department at the Faculty of Science at the University of Tromsø.

I want to thank my team members – both current and former; Jeanet Conradie, Ingar Wasbotten and Hege Ryeng for scientific and aesthetical discussions, Kathrin Hopmann for buffering and proofreading and Emmanuel Gonzalez for providing useful references. I would like to thank my supervisor Prof. Abhik Ghosh for introducing me to bioinorganic chemisty and opening my eyes towards the field of science. Also, being a part of CTCC has been a great inspiration, and also, more importantly (to me), great fun.

I want to thank Prof. Peter R. Taylor for having me as a visitor in his laboratory. Thank you Pete, Nat, Kaz, Matt, Dave, Dev and all the other super-nice people I met in Warwick!

During the time of my PhD I have been a significant consumer of computer time, and the support staff at the IT center at UiT, in particular Roy Dragseth and Steinar Trældal-Henden, are gratefully acknowledged for their advice and patience. Financial support and computer time was granted by the Research Council of Norway (NFR), both of which I acknowledge gratefully.

My warmest gratitude goes to Brita, who has endured my shifting moods and frustration in the finishing process. I love you!

Tromsø, September 2008

Espen Tangen

LIST OF INCLUDED PAPERS

The papers are ordered chronologically:

1. Tangen, E.; Svadberg, A.; Ghosh, A. "Toward Modeling H-NOX Domains: A DFT Study of Heme-NO Complexes as Hydrogen Bond Acceptors," *Inorganic Chemistry* **2005**, *44*, 7802-7805.

2. Tangen, E.; Conradie, J.; Ghosh, A. "The Challenge of Being Straight: Explaining the Linearity of a Low-Spin $\{FeNO\}^7$ Unit in a Tropocoronand Complex," *Inorganic Chemistry* **2005**, *44*, 8699-8706.

3. Conradie, J.; Tangen, E.; Ghosh, A. "Trigonal bipyramidal iron(III) and manganese(III) oxo, sulfido, and selenido complexes. An electronic-structural overview," *Journal of Inorganic Biochemistry* **2006**, *100*, 707-715.

   Comment: My contribution to this work was the oxo complexes.

4. Tangen, E.; Conradie, J.; Ghosh, A. "Bonding in Low-Coordinate Environments: Electronic Structure of Pseudotetrahedral Iron-Imido Complexes," *J. Chem. Theory Comput*. **2007**, *3*, 448-457.

Reprints were made with permission from the copyright holders.

ABBREVIATIONS AND ACRONYMS

MO = Molecular Orbital

R = organic molecule Residue (or substituent).

HF = Hartree-Fock

SCF = Self Consistent Field

TBP = Trigonal BiPyramidal

SQP = SQuare Pyramidal

CFT = Crystal Field Teory

TMC = Transition Metal Complexes

LCAO = Linear Combination of Atomic Orbitals

AO = Atomic Orbital

LFT = Ligand Field Theory

HOMO = Highest Occupied Molecular Orbital

LUMO = Lowest Unoccupied Molecular Orbital

(Por) = Porphine

ImH = Imidazole

SOMO = Singly Occupied Molecular Orbital

TC = TropoCoronand

TBP_{eq} = TBP with the NO-group in the equatorial postion

TBP_{ax} = TBP with the NO-group in the axial position

(tam) = Tropo AmiMinato

(me_2tam) = DiMethyl-tam

EAN = Effective Atomic Number rule

MEC = Maximum Electron Count

Im = Imido

Ar = Aryl

OEP = ß-OctaEthyl-Porphyrin

TABLE OF CONTENTS

1 INTRODUCTION

Many life-critical processes require metal ions, including respiration, nitrogen fixation, photosynthesis, nerve transmission and muscle contraction.[1] The role of the metal varies across structural to catalytic. Transition metal ions have a rich chemistry due to close-lying energy bands made up of partly filled d-orbitals, and thus serve as unique agents in a variety of biological processes. In particular, this is the case for the middle and late first-row transition metal ions, with typically single occupation of at least some of their d-orbitals. For these elements, tuning the ligand field by the use of different ligands provides a useful way of influencing structure, spin state and bond-order. Unperturbed Fe^{III} and Mn^{II} ions would typically be high-spin d^5, but in bioinorganic complexes ions display all possible spin states from S = 1/2 to S = 5/2. In essence, local structure about the metal plays an essential role for catalytic mechanisms.

From the many beautiful studies of bioinorganic systems, synthetic, structural, spectroscopic or computational, principles have emerged that tie together seemingly unrelated facts.[1] In this work, search for such facts is the primary aim. On the basis of a thorough MO description of selected molecules, we have derived general concepts about bonding patterns in low-coordinate middle and late first-row transition metal nitrosyl and imido complexes.

The general interest in iron- and manganese imido and nitrosyl complexes stems partly from the fact that identical or similar compounds have significant roles in biology.[2, 3] The field of transition metal nitrosyls, referring to structural and bonding aspects, was termed a provocative subject by Enemark and Feltham[4] in their ground-breaking work from early 70ties. Possibly less provocative today, the field is still of significant interest.

In this thesis, calculations on 4- and 5-coordinate transition metal imido and nitrosyl complexes will be presented. The complexes studied include pseudotetrahedral-, square pyramidal- and trigonal bipyramidal coordination geometries, with either apical or equatorial NX (X being either O or R) ligands, about the metal ion. The main tool of this thesis is

Density Functional Theory (DFT), which has proved itself a quite reliable tool in the area of bioinorganic chemistry.[5] The primary aim of this study is to examine the geometric and electronic structure of low-coordinated first-row transition metal nitrosyl and imido complexes. MO arguments derived from these examinations should lead to conclusions about the bond structure of low-coordinate complexes in general.

Before presenting the main conclusions in **Chapter 5**, a brief introduction to computational chemistry methods is presented in **Chapter 2** and a brief introduction to structural theories is presented in **Chapter 3**. **Chapter 4** presents a general overview of low-coordinate transition metal monoimido or –nitrosyl complexes, including our results reported in **Papers 1-4.**

2 COMPUTATIONAL CHEMISTRY

Computational modeling of molecules is a quite accurate method for predicting molecular properties such as geometric and electronic structures, frequencies and relative energies. One of its strengths is the opportunity to study species, processes and/or conditions that are difficult to obtain in a lab. Obtaining the potential energy surface of a molecule, the electron distribution of a short-lived intermediate, the energy differences of structural isomers and molecule orbital occupation in radicals are examples of such.

In computational quantum chemistry, the applied models are given by quantum mechanics. Originally, computational quantum chemistry suffered from severe limitations with respect to the size of molecules possible to investigate. The development of more efficient computers and more elaborate mathematical tools has overcome parts of this limitation, thus enabling researchers to look at real- or almost real-sized systems. However, because computational chemistry methods employ a number of approximations, and often neglect effects such as solvent or relativistic effects, the results obtained from computational calculations should always be treated with some degree of caution.

2.1 BASIC QUANTUM CHEMISTRY

In quantum mechanics, the state of a system is described by a wavefunction. The wavefunction gives all possible information about the system.[6] To gain knowledge about possible future states of a quantum mechanical system from its present state, we want an equation that tells us how the wave function changes with time and space.

For time-independent systems, the time-dependent part may be factored out, and we get the equation known as the time-independent Schrödinger equation, named after its discoverer, Austrian physicist Erwin Schrödinger. For a single particle system it is:

$$-\frac{\hbar^2}{2m}\frac{d^2\psi(x)}{dx^2}+V(x)\psi(x)=E\psi(x)$$

More generally written as:

$$H\Psi(x) = E\Psi(x)$$

where Ψ denotes the molecular wave function, E the total energy of the state and H the Hamiltonian operator. The Hamiltonian operator contains the kinetic and potential energy terms for the whole system. Once the correct wavefunction is known, it is in principle possible to extract all information about the system. Unfortunately, it is only possible to solve the Schrödinger equation exactly for one- and two particle systems. And because of this, a variety of methods for obtaining approximate solutions have been developed. These methods range from methods having adjusted parameters (semiempirical methods) to highly advanced analytical methods based on different mathematical formalisms (coupled cluster, configuration interaction, many-body perturbation theory).

Since the electrons are significantly lighter than the nucleus, they will act differently according to molecular motion. When the nuclei change their configuration slightly, electrons immediately will adjust. This difference in behavior leads to a possible separation of the wavefunction in an electronic and a nuclear part:[7]

$$\Psi_{tot}(q_{el}, q_{nuc}) = \Psi_{el}(q_{el}; q_{nuc}) \bullet \Psi_{nuc}(q_{nuc})$$

This is called the Born-Oppenheimer approximation. Here q_{el} and q_{nuc} denote the electronic and nuclear coordinates, respectively. The formalism $(q_{el};q_{nuc})$ indicates that the electronic coordinates are parametrically dependent on the nuclear coordinates. In practice, the Born-Oppenheimer approximation implies that the electronic wavefunction can be solved in a stationary nuclear framework.

The Variational Principle states that an approximate wavefunction has an energy which is above or equal to the exact energy, E_0:[7, 8]

$$\frac{\int \Phi \hat{H} \Phi d\vec{r}}{\int \Phi^2 d\vec{r}} \geq E_0$$

The equality only holds if the wavefunction is exact, providing a powerful tool for solving the wavefunction. As long as the energy keeps dropping, one is on the right track.

For a single-electron system, the eigenfunctions of the electronic Schrödinger equation can properly be called molecular orbitals. If the system only has one nucleus, the equation can be solved exactly, and the eigenfunctions would be hydrogen-like atomic orbitals. Naively, one could think that these atomic orbitals or a linear combination of them would serve as a decent starting point for constructing more complicated molecular orbitals. We would then construct a starting guess wave function as a linear combination of atomic wave functions φ;

$$\phi = \sum_{i=1}^{N} a_i \varphi_i$$

where the set of N functions φ_i comprise the basis set, each φ_i associated with some coefficient a_i. This construction is called the linear combination of atomic orbitals (LCAO), a fundamental approach in quantitative molecular orbital theory.[7]

The charge density

$$\rho(\vec{r}) = \sum_{\mu} \sum_{\nu} P_{\mu\nu} \phi_{\mu}(\vec{r}) \phi_{\nu}^{*}(\vec{r})$$

where P denotes the density matrix, represents the probability of finding an electron in various regions of space and is commonly pictured by contour maps for various planes drawn through the molecule. [9] There is no unique definition of the number of electrons to be associated with a given atom or nucleus in a molecule, but it is sometimes useful to perform such population analysis.[9] By substituting the basis expansion of ψ_a into the equation that divides the total number of electrons into two electrons per molecular orbital;

$$N = 2 \sum_{a}^{N/2} \int d\vec{r} \, | \psi_a(\vec{r}) |^2$$

we have;

$$N = \sum_{\mu} \sum_{\nu} P_{\mu\nu} S_{\nu\mu} = \sum_{\mu} (PS)_{\mu\mu}$$

where S denotes the overlap matrix, and it is possible to interpret $(\mathbf{PS})_{\mu\mu}$ as the number of electrons to associated with ϕ_μ. This approach is called the Mulliken population analysis. Assuming the basis functions are centered on atomic nuclei, the corresponding number of electrons to be associated with a given atom in a molecule is obtained by summing over all basis functions centered on that atom.

2.2 WAVEFUNCTION-BASED METHODS

Ab initio means "from the origin" in Latin and denotes wavefunction-based methods. The simplest qualitative model is the Hartree-Fock (HF) approximation. Here the N-body wavefunction is be described by a single Slater determinant of N spin orbitals. The method is also called the self-consistent field method (SCF). In this model, each particle is assumed to experience a mean field created by the other particles. The HF method accounts for a large part of the electron-electron interaction, including the exchange energy. The difference between the exact energy and the approximate HF energy is named the correlation energy. To account for the correlation energy several different approaches are in use. This is the major resource-consuming step in ab initio calculations. Some of these methods are mentioned in Table 1.

Table 1. A brief description of electronic structure calculation methods. Adapted from reference 10.

Method	Description	Performance on accuracy
SCF	Orbital approximation for a single-electron configuration	Modest for structures and vibrational frequencies, poor for energetics.
MP2	Improvement on HF using perturbation theory.	Good for structures and frequencies, modest for energetics.
CCSD(T)	Improvement of HF theory including excited Slater determinants in the wavefunction.	Excellent for structures, frequencies and energetics when a single electronic configuration is a good initial approximation.
CASSCF	Wavefunction approximation using multiple electron configurations.	Modest to reasonably good for structures, frequencies and energetics.
CASPT2	Improvement of CASSCF theory using second order perturbation theory.	Good structures and frequencies, good excitation energies, reaction energies of modest accuracy.
DFT	Density-based methods with parameterized exchange and correlation.	Good structures and frequencies; more variable on energetics significantly dependent on the functional used.

In both the HF and DFT formalisms the wavefunction is represented by a determinant of one-electron functions (orbitals). If we use a complete set of orbitals, the solution of the Schrödinger equation would yield the exact single determinant representation, and

representing the wavefunction as an expansion in a complete basis of determinants would yield the exact solution of the wavefunction within the Born-Oppenheimer approximation. This is a powerful concept, because increasing the number of basis functions generally would improve the accuracy of the models, and this generally holds well for molecular modeling. However, in some cases there are needs for having a multi-determinental representation, and this is often the case for transition metals.[11] In the more troublesome cases DFT and single-determinental *ab initio* fails equally.

Table 2. Formal scaling behavior as a function of basis functions N of various electronic structure methods. Adapted from reference 7.

Scaling behavior	Method(s)
N^4	HF
N^5	MP2
N^6	MP3, CISD, MP4SDQ, CCSD, QCISD
N^7	MP4, CCSD(T), QCISD(T)
N^8	MP5, CISDT, CCSDT
N^9	MP6
N^{10}	MP7, CISDTQ, CCSDTQ

2.3 DENSITY FUNCTIONAL THEORY

The foundation of Density Functional Theory is the idea that the energy of the electron can be written in terms of the electronic probability density, ρ. For a system of n electrons, ρ(**r**) denotes the total electron density at a particular point **r** in space. The electronic energy E is said to be a functional of the electron density, denoted E[ρ(**r**)], indicating that for a given function ρ(**r**) there exist a single corresponding energy.[12]

Kohn and Sham made DFT available for computational chemistry by introducing the concept of a non-interacting reference system built on one-electron functions.[13] The Hamiltonian for this system will have eigenvalues that are simply the sum of the one-electron eigenvalues.[7] The crucial bit of cleverness is, as always, to choose the proper fictitious system to generate the ground state density from. Then the energy expression is divided into specific components to facilitate further analysis:

$$E_{DFT}[\rho] = T_{ni}[\rho] + V_{ne}[\rho] + V_{ee}[\rho] + E_{xc}[\rho]$$

Here T_{ni} symbolizes the exact kinetic energy of a non-interacting system, V_{ne} is the potential energy generated by the interaction between electrons and nuclei, V_{ee} is the potential energy generated by the interaction between electrons (the Coulomb energy) and the last term includes the correction term for the kinetic energy deriving from the interacting nature of the electrons and all the non-classical corrections to the electron-electron repulsion energy, conveniently lumped together in one exchange-correlation energy term.

As we see from the formula above, the kinetic energy of the non-interacting reference system, the attraction between electrons and nuclei and the Coulombic repulsion between electrons are calculated exactly in the Kohn-Sham approach. Unfortunately, the Hohenberg-Kohn theorems do not state the relationship between the functional and the density.[14] Thus, for a given density, the exchange-correlation part is unknown and the challenge in DFT is to design a functional that models E_{xc} well and a usual approach is to handle the exchange part and the correlation part separately.

The model functionals in use may be divided into three different subgroups; the local density approximations, the gradient corrected approximations and the hybrid functionals. A local density approximation computes the value of ε_{xc} (the approximated value of the exchange-correlation term) at the position $\mathbf{r}$ exclusively from the local density $\rho(\mathbf{r})$. Typically the density is treated as a uniform electron gas, and the approximation may account for spin polarization. In a gradient corrected approximation, the gradient of the electron density is also taken into account, to adjust for the general non-uniform electron density case. The hybrid functionals are named so because a part of the exchange contribution is taken from a Hartree-Fock method calculation and parameterized into the functional.

The greatest advantage of DFT compared to *ab initio* calculations is the low computational cost, especially for large systems. On the other hand, it is not possible to carry out systematic improvement by taking more electron configurations into account, which you can do for *ab initio* methods. The only way to improve the result is to use better functionals. Furthermore, the typical functional is designed with respect to first and second-row elements.

Performance of DFT in the Bioinorganic Area

Most computational studies of transition metal complexes with relevance to biology have been carried out using DFT methods.[10, 15, 16] With large molecular sizes and often more than one open-shell transition metal center, bioinorganic problems are generally too demanding for high level *ab initio* calculations such as CASPT2 and CCSD(T).[5] On the other side, DFT has performed well on bioinorganic problems because this method handles larger systems with comparable accuracies for a fraction of the computational cost compared to *ab initio* methods.[5, 10] However, for DFT calculation results on open-shell transition metal systems there are several known cases of imperfectly described systems.[17] A recent report on the performance and limitations of DFT assigns these errors to the delocalization error of approximate functionals from the dominating Coulomb-term and imperfect description of static correlation in DFT.[11] The latter would typically give large errors for situations with degeneracy or near-degeneracy – as is often the case in transition metal chemistry.

For transition metal porphyrins, DFT is known to provide reasonable to good structures.[15] For relative energies of low-lying electronic states, however, DFT displays more variable performances. As mentioned above, the exchange part of the electron-electron interaction is described in an approximate way using functionals in DFT, and this may be one cause to the problem.[10] The exchange part describes correlation between electrons of the same spin and is important when discussing relative energies of different electronic states in open-shell systems. Consequently, a precise description of the exchange is of particular importance when the states of interest have a different number of unpaired electrons. In *ab initio* methods, the exchange is handled exactly, thus high-quality *ab initio* methods, CCSD(T) and CASPT2 are found to describe the relative energies of low-lying states more accurately than DFT for transition metal complexes.[10, 17] And this indicates the value of validation of DFT results versus corresponding high level *ab initio* method investigations.[18] Unfortunately, only a few such studies have been carried out.

The application of quantum chemical methods to challenges in bioinorganic chemistry today is extensive,[17, 19] with corresponding need for validation. Quite recently, a few such papers have appeared – concluding that DFT is an accurate and efficient way to describe ground state

energetics of bioinorganic compounds. [17, 19, 20, 21, 22] However, the errors in relative energies vary between a couple of tenths of an eV and up to almost 1 eV,[10, 20] proving the need of individual assessment.

MO arguments are a widely used conceptual tool in inorganic chemistry, and work by Baerends firmly establishes the Kohn-Sham MOs as physically meaningful entities.[23] Both theoretical arguments and experimental investigations show that an analogue of Koopman´s theorem applies to the Kohn-Sham MOs.[24, 25] Thus, we are fairly confident that the MO arguments in this thesis will hold.

2.4 COMPUTATIONAL DETAILS OF PRESENTED WORK

The choice of software and functionals is primarily pragmatically founded: The method of DFT/PW91 was chosen after considering computational costs, performance and availability. All the work presented in this thesis is carried out with various versions of the ADF program package[26] and most of the graphics has been provided using the ChemCraft graphical software package.[27]

A majority of the calculations were performed using the PW91[28] functional for both exchange and correlation together with triple-ζ basis sets, a very fine integration mesh and tight criteria for self consistent field convergence and geometry optimization. As a check on the performance of the PW91 functional, some calculations were performed with the optimized Becke (B88) exchange functional (OPTX)[29] together with the Lee, Yang and Parr (LYP)[30] correlation functional. The latter combination is generally termed OLYP, and we are increasingly favoring it for transition metal applications.

Where hybrid functional energies and/or surveys of functionals are presented, the noniterative post-SCF energies are computed on basis of the previously optimized PW91 or OLYP geometries using the HFEXCHANGE and METAGGA keywords in ADF.[26] For reference to the functionals used, see the ADF package reference list.[31] Some of these references are also encountered in our Paper 3. For the work presented in our Paper 1, the energies associated with hydrogen bonding were corrected for basis-set superposition error (BSSE) by the counterpoise method. Since our work generally has been focusing on electronic structures and

conceptual aspects of bonding, the performance of DFT methods compared to alternative methods has not been heavily evaluated.

3 FUNDAMENTAL STRUCTURAL CONCEPTS

3.1 INTRODUCTION TO TRANSITION METAL COORDINATION

The variety of transition metal compounds stems from the diversity of available oxidation states for the metal ions and their ability to form complexes with a wide range of ligands,[32] giving a wide range of coordination numbers and geometries.[33] The term transition metal is generally restricted to that of an element with at least one ion with an incomplete outer set of d-electrons, and for the first-row transition metals, all valence electrons on the metal are regarded as d-electrons when the metal is in a complex. Transition metal complexes comprise of transition metal ions covalently bonded to other ions or molecules, generally termed ligands.

Structures of Coordination Compounds

Coordination number 3

The most symmetrical 3 coordinate arrangements are planar (having D_{3h} geometry) and pyramidal (having C_{3v} geometry). This coordination number is rare for metal complexes, because nearly all MX_3 metal complexes have structures where sharing of ligands leads to a higher coordination number for metal. A few exceptions are known, including the MN_3 group that occur in $Cr/Fe(NR_2)_3$.[34]

Coordination number 4

There are three principal geometries for 4-coordinate complexes; the tetrahedral geometry (with symmetry T_d), the square planar geometry (with symmetry D_{4h}) and the irregular arrangement of symmetry that may occur when a ligand in a trigonal bipyramidal (TBP) arrangement is replaced by a lone pair of electrons. The square planar arrangement typically occurs in many transition metal complexes because of the presence of additional valence shell electrons. A substitution of one of the ligands in a tetrahedral geometry typically gives

pseudotetrahedral arrangements with local symmetry C_{3v} about the metal ion, as seen for the iron imido complexes studied in Paper 4.

Coordination number 5

For 5-coordinate complexes, there are two principal geometries; the trigonal bipyramidal (TBP) arrangement (having D_{3h} symmetry) and the square pyramidal (SQP) arrangement (having C_{4v} symmetry) (see Figure 1 and Figure 2). For the TBP arrangement, a substitution of one of the axial ligands typically would lower the symmetry to C_{3v} whereas a substitution of one of the equatorial ligands would lower the symmetry to C_{2v}. Pentagonal planar coordination, where two ligands are bidentate and one monodentate, is very unusual and seems to be due to the presence of two stereochemically active lone pairs.[34]

Coordination number 6

There are three principal forms of distortion of an octahedron. The tetragonal distortion (symmetrical distortion along one C_4 axis) gives D_{4h} symmetry, the rhombic distortion (unsymmetrical distortion along one C_4 axis) gives D_{2h} symmetry and the trigonal distortion gives D_{3d} symmetry. The tetragonal distortion most commonly involves an elongation of one C_4 axis and in the limit two trans ligands are lost completely, leaving a square planar 4-coordinate complex.[34]

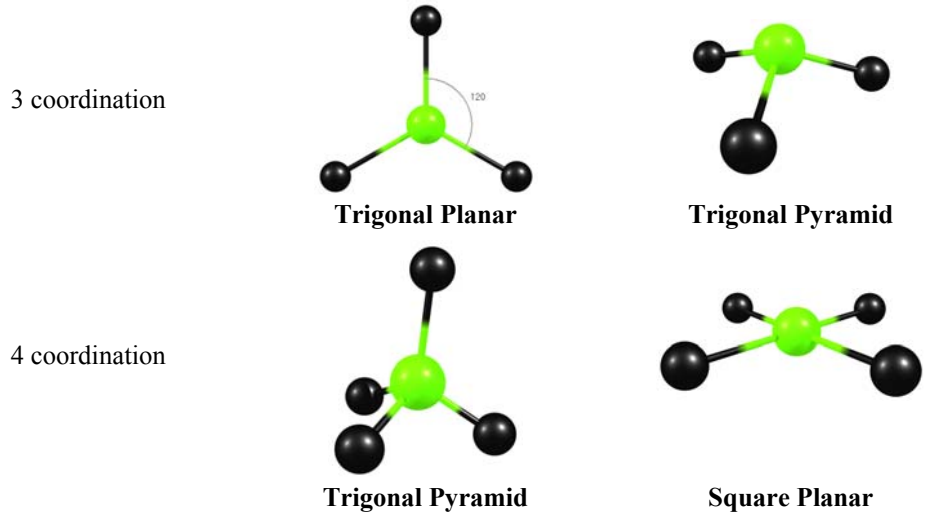

Figure 1. Typical geometries for 3 and 4 coordinate complexes. Adapted from Lippard and Berg.[1]

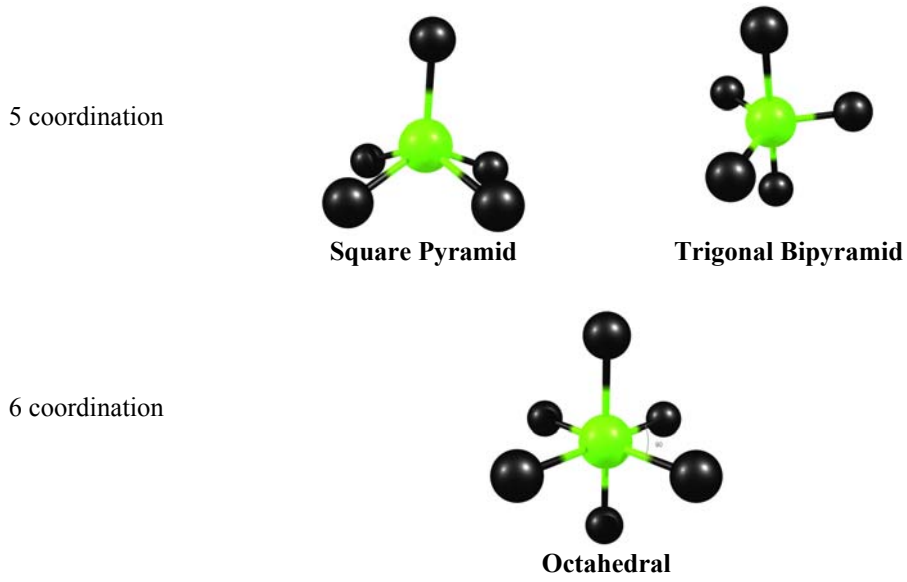

Figure 2. Typical geometries for 5 and 6 coordinate complexes. Adapted from Lippard and Berg.[1]

3.2 INTRODUCTION TO CRYSTAL FIELD THEORY

Crystal Field Theory (CFT) is a purely electrostatic approach to the electronic structure of transition metal complexes (TMC). In CFT, the ligand lone pair is modeled as a point negative charge or as the part negative charge of an electric dipole that repels electrons in the *d*-orbitals of the central metal ion. CFT focuses on the resultant energy splitting (termed the crystal field splitting parameter) of *d* orbitals into groups and then uses that splitting to account for the number of unpaired electrons in transition metal complexes. Even though this theory ignores covalent bonding interactions between ligands and central metal ions in transition metal complexes, it provides a remarkably good qualitative explanation of many of their properties.[35, 36]

The Crystal Field splitting is affected by the following factors:

- the nature of the metal ion.
- the metal's oxidation state. A higher oxidation state leads to a larger splitting.
- the geometrical arrangement of the ligands around the metal ion.
- the nature of the ligands surrounding the metal ion. The stronger the effect of the ligands the greater the difference between the high and low energy 3*d* groups.

Octahedral Coordination Complexes

The splitting of the d-orbitals for a metal ion in an octahedral field serves as a good illustration of CFT. Overall in a complex, all the d-orbitals are elevated in energy relative to a free ion state. But because the ligands are typically oriented along the axis in a Cartesian system for 6-coordinate octahedral complexes, the electrons in the orbitals pointing along the axes (usually d_{z^2} and $d_{x^2-y^2}$) are repelled more than those in the orbitals pointing between the axes (usually d_{xy}, d_{yz} and d_{zx}). The former are raised in energy, the latter are lowered relative to the spherical distribution and the energy of the two doubly degenerate (e_g) orbitals (the d_{z^2} and the $d_{x^2-y^2}$) must be raised 1.5 times as much as the three triply degenerate (t_{2g}) orbitals (the d_{xy}, d_{yz} and d_{zx}) are lowered in order to maintain balance. This is termed the Barycentre rule.

For a complex in an octahedral ligand field, CFT assigns the first absorption maximum in the electronic spectrum to the transition $e_g \leftarrow t_{2g}$. For complexes with more than one *d*-electron the energy of transition depends on repulsion energies between the *d* electrons also, and the picture gets a bit more complicated.

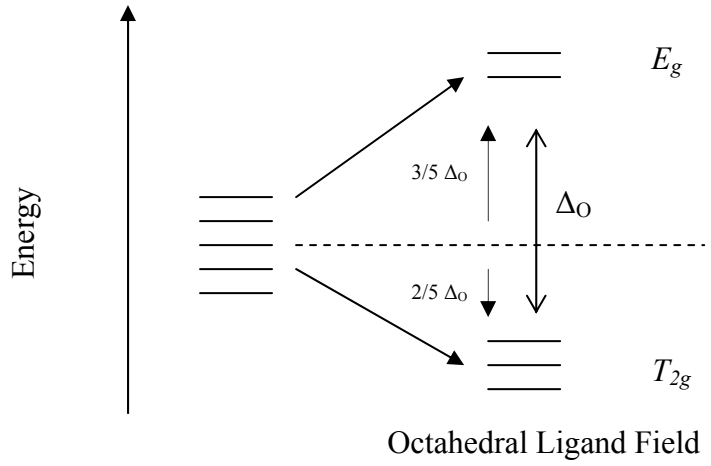

Figure 3. The separation of the orbitals into two sets is called a crystal-field splitting parameter Δ, where a subscript O signifies octahedral complexes.

Tetrahedral Coordination Complexes

For the tetrahedral geometry, the negative charges of the ligands lie between the coordinate axes, and electrons in the d_{xy}, d_{yz} and d_{zx} orbitals are repelled more than those in the d_{z^2} and $d_{x^2-y^2}$ orbitals. None of the orbitals points directly at the negative charge and the separation of the

two sets of orbitals are much smaller than in an octahedral ligand field. In Figure 4 the CFT splitting is shown for a variety of relevant coordination geometries, including the tetrahedron-derived pseudotetrahedral C_{3v} symmetry. Most tetrahedral complexes are high-spin, with notable exceptions studied in this work (Paper 4).

Crystal Field Strength and Electron Distribution

When there is no competition between the crystal field splitting parameter Δ and the pairing energy E_p (the Coulombic repulsion between two electrons in an orbital), the ground state electron configuration is unambiguous (typically octahedral d^3 complex). When alternative configurations are possible, the distinction between high- and low-spin configurations is decided by the size of the E_p relative to Δ.

Because the Δ-value depends on both the metal and the ligands, and the spin pairing energy varies with the metal, the decision between high- and low-spin configurations is not always easy.

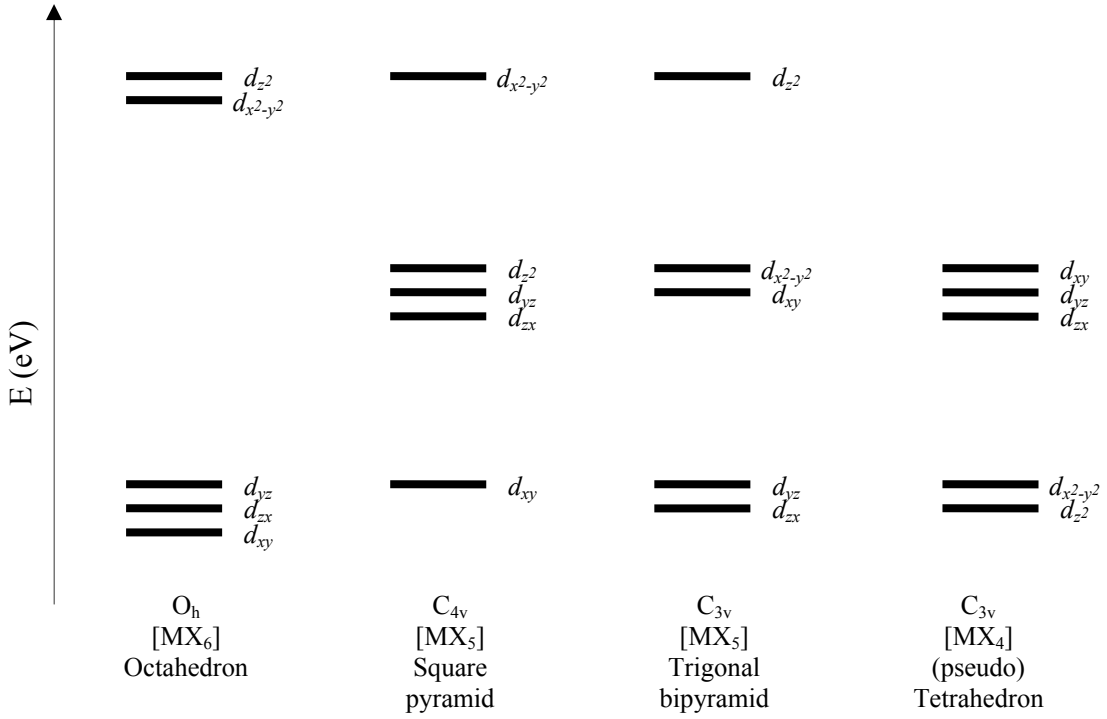

Figure 4. Crystal field splitting diagrams for relevant coordination geometries. The vertical energy axis is schematic.

3.3 INTRODUCTION TO MOLECULAR ORBITAL THEORY

Molecular Orbital Theory (MO theory) is a method for determining molecular electronic structure by applying the orbital theory that holds for atoms onto molecules. In MO theory, electrons are not assigned to individual bonds, but are treated as moving under the influence of the nuclei in the whole molecule. In this theory each molecule has a set of molecular orbitals. It is assumed that the molecular orbital wave function ψ_j may be written as a simple weighted sum of the n constituent atomic orbitals χ_i, according to the following equation;[8]

$$\psi_j = \sum_{i=1}^{n} c_{ij} \chi_i$$

where the C_{ij} are coefficients that may be determined numerically, by substituting this equation into the Schrödinger equation and applying the variational principle.

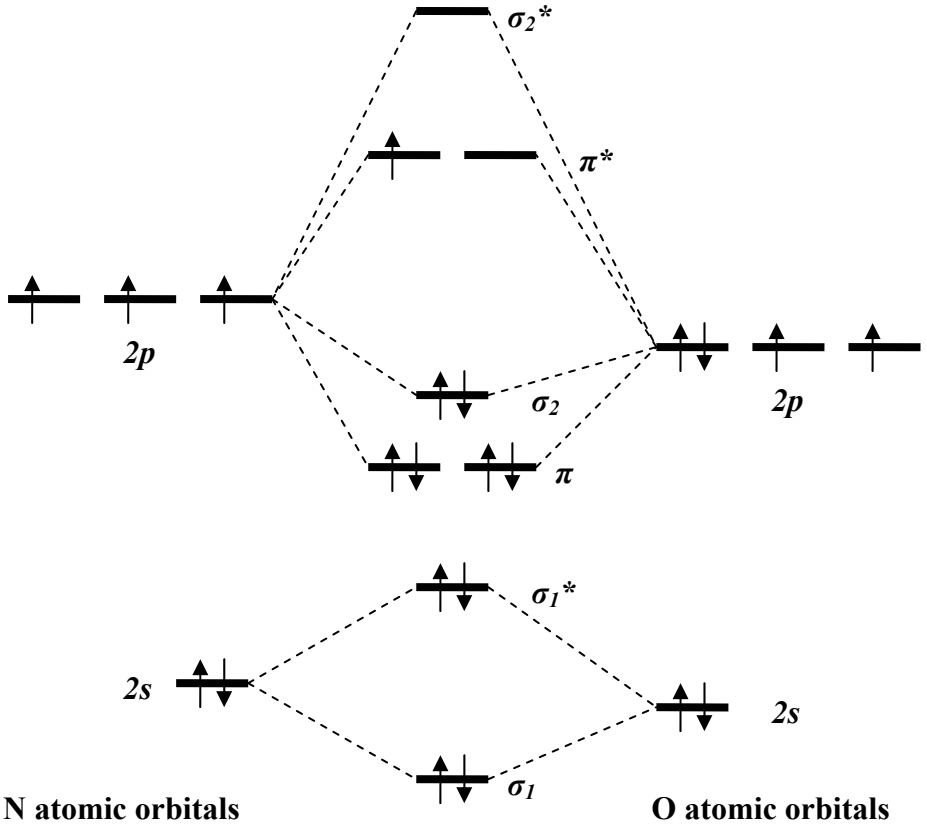

Figure 5. Qualitative MO diagram for NO. Adapted from McCleverty.[37]

A molecular orbital (MO) specifies the spatial distribution and energy of one or one pair of electrons, most commonly an MO is represented as a linear combination of atomic orbitals from the atoms comprising the molecule (the LCAO approach). For diatomics this is easily feasible, but for larger molecules this becomes increasingly complicated and is done by computers. Applied onto chemical problems, the MOs are divided into bonding orbitals, nonbonding orbitals and antibonding orbitals. The former represents a lower energy constellation than the parentage AOs, the latter a higher energy constellation. In principle molecules will form bonds if the atomic orbital MO combination becomes lower in energy than the AO combination. The qualitative MO model provides a simple description of bonding structures in molecules, and thus is a useful tool in applied computational chemistry.

Introduction to Ligand Field Theory

To overcome the conceptual weaknesses of CFT, **Ligand Field Theory** (LFT) was created as a combination of CFT and MO theory. For instance the metal-ligand charge transfer (MLCT), being hard to explain by regarding the ligands as negative point charges, is now regarded in light of possible metal-ligand orbital overlaps and thus more conceptually feasible for LFT. LFT also describes the bonding in coordination complexes by regarding the metal d-orbitals and their energy levels relative to each other. The key idea is that orbitals with the same symmetry can overlap.

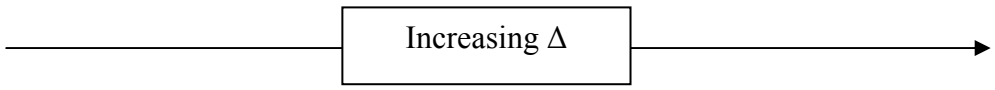

π donor < weak π donor < no π effect < π acceptor

Figure 6. Schematic illustrating how π-donating abilities of the ligands affects the ligand field splitting parameter.

For instance σ bonding is made up by an orbital overlap between ligand orbitals and metal ion orbitals with σ symmetry respective to the metal-ligand (M-L) bond axis. The classification of orbitals into σ, π and δ follows from the irreducible representation of the $C_{\infty v}$ point group, where the bond axis contains the highest order rotation axis (C_∞). Likewise, π bonding is made up by M-L π-orbital bonding overlap. A ligand with filled π-symmetry orbitals energetically similar to the metal π-symmetry *d* orbitals, would, if having no low energy

vacant π orbitals, donates electrons to these metal orbitals and creates a bond. This donation is depending on available empty or partly empty metal d_π orbitals. The M-L bond is somewhat strengthened by this interaction, but the complementary antibonding MOs are typically comparable in energy to the σ anti-bonding MO. They are filled with electrons from the metal *d*-orbitals, when available, to become the HOMOs of the complex. For that reason, Δ decreases when ligand-to-metal π- bonding occurs.

Oppositely, a π acceptor ligand has usually empty π-symmetry orbitals, typically vacant antibonding orbitals, lower in energy than metal π-symmetry *d* orbitals, available for occupation. One important π-bonding interaction in coordination complexes is the π-backbonding. This typically occurs when the ligand LUMOs are π* orbitals and they couple with metal d_π orbitals to form bonds. This is strengthening the metal-ligand bond and increasing the Δ. The corresponding antibonding orbitals are higher in energy than the σ-antibonding orbital, and the ligands end up occupying their π* orbitals and by that weakening the bond within themself.

4 LOW-COORDINATE IMIDO AND NO COMPLEXES

4.1 LOW COORDINATE NITROSYL COMPLEXES

Introduction to Nitrogen Chemistry

For atomic nitrogen in its ground state, the electronic configuration is $1s^2 2s^2 2p^3$, where the three 2p electrons are distributed with parallel spin among the p_x, p_y and p_z orbitals, and the nitrogen atom can complete its octet in several ways:

- Form the nitride ion (N^{3-}) by electron gain.
- Form electron-pair bonds, either single bonds as in NH_3 or multiple bonds as in N_2.
- Form electron-pair bonds with electron gain, like in the imide ion (NH^{2-}).
- Form electron-pair bonds with electron loss, like in ammonia (NH_4^+). These ions, with the general formula R_4N^+ may be regarded as formed by protonation of the nitrogen atom lone pair.

There are a few stable nitrogen species with incomplete octet, and the classical example is NO, which has one unpaired electron in a π^* orbital.

Nitric Oxide - The Molecule and Ligand

Nitric Oxide is a stable free radical, the molecular orbital diagram (Figure 5) showing that the unpaired electron in this molecule resides in a π^* molecular orbital. The bond length of free NO is 1.154 Å, being between that of a double (1.18 Å) and a triple (1.06 Å) bond. Convention regards this bond length as equivalent to a bond order of 2.5, consistent with the MO diagram (Figure 5).

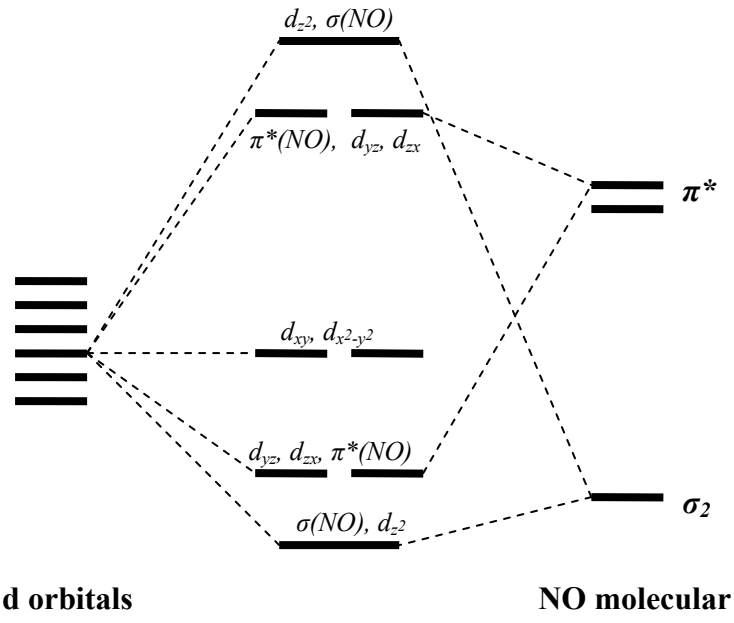

Figure 7. Qualitative Metal-NO unit orbital diagram for a hypothetical linear MNO unit. The NO σ_1, σ_1*, π are so much lower than the metal d-orbitals in energy, so that they do not interact. The NO σ_2* is so much higher than the metal d-orbitals in energy so that they do not interact. Based on single point DFT/OLYP calculations.[38]

Just as the CO group (which is isoelectronic with NO^+), the NO group reacts with a metal atom that presents an empty σ orbital and a pair of filled d_π orbitals to give a linear MNO unit with a X → M σ bond (the (σ(NO), d_{z^2}) combination in the MO scheme in Figure 7, illustrated graphically in Figure 8) and M → X π bonding (shown in Figure 8).

Figure 8. The metal d-orbital - NO π- (to the left) and σ-bonding (to the right) interactions. Adapted from McCleverty.[37]

The reaction between the metal and the NO group may, at least formally, be regarded as involving an empty σ orbital and a pair of d_π orbitals containing three electrons. Thus, the full four electron metal dπ → NO π* interaction is made up of three electrons from the metal and one from NO, and NO is regarded as a $3e^-$ donor.[34, 37]

The Enemark-Feltham Electron Count

Due to the difficulty of assigning formal oxidation states to the metal and the NO in nitrosyl complexes arising from the covalent nature of the M-N-O interaction, Enemark and Feltham proposed a formalism which treated the metal nitrosyl as an inorganic functional group unit.[39] This unit was represented as $\{MNO\}^n$, where n is the total number of metal d-electrons plus the number of electrons in NO exceeding those on NO^+. The number of metal d electrons is determined by the formal oxidation state of the metal atom, assuming no charge on the NO. This formalism makes no assumption of the actual distribution of electrons between the metal and the NO group and also makes no assumption about the M-N-O angle.

Geometry of NO Complexes

In the traditional picture, the metal-NO bonding is achieved by the NO lone pair filling into the empty metal d_{z^2} orbital and by backbonding through the overlap between the two metal d_π orbitals and the NO π^* orbitals.[40] Terminal nitrosyl ligands may adopt either linear or bent M-N-O geometries. Relatively few complexes have truly linear arrangements, so generally MNO units with M-N-O angles in the range of from 160° to 180° are still regarded as linear.[34] Truly bent MNO-groups have MNO bond angles between 120° and 150°.

Transition Metal Nitrosyl Complexes

The Structure of MNO Units according to Enemark and Feltham

The diagrams in Figure 9 were constructed from the metal d- and the NO π^* orbitals, which molecular orbital calculations have shown to be similar in energy and strongly interacting.[41] Because the NO ligand is a strong π-accepting ligand,[42] the (d_{xz}, d_{yz}, π^*(NO))-orbitals are shown as the lowest MOs in all of the diagrams of Figure 9. These orbitals are bonding with respect to M and N, but antibonding with respect to N and O. The (d_{xy}, $d_{x^2-y^2}$) orbitals are non-bonding in $C_{\infty v}$ symmetry, and the (d_{z^2}) orbital is σ-antibonding with respect to M and N. Finally, the (π^* (NO), d_{xz}, d_{yz}) orbitals are antibonding with respect to M, N and O. As seen from the Figure 9, where the (π^*(NO), d_{xz}, d_{yz}) and (d_{z^2}, σ (NO)) orbitals represent the antibonding metal-NO interactions, we only need to consider the relative ranking of the

(π^*(NO), d_{xz}, d_{yz}) orbitals with respect to the other orbitals to decide whether a given value on n will produce a linear or bent MNO unit.

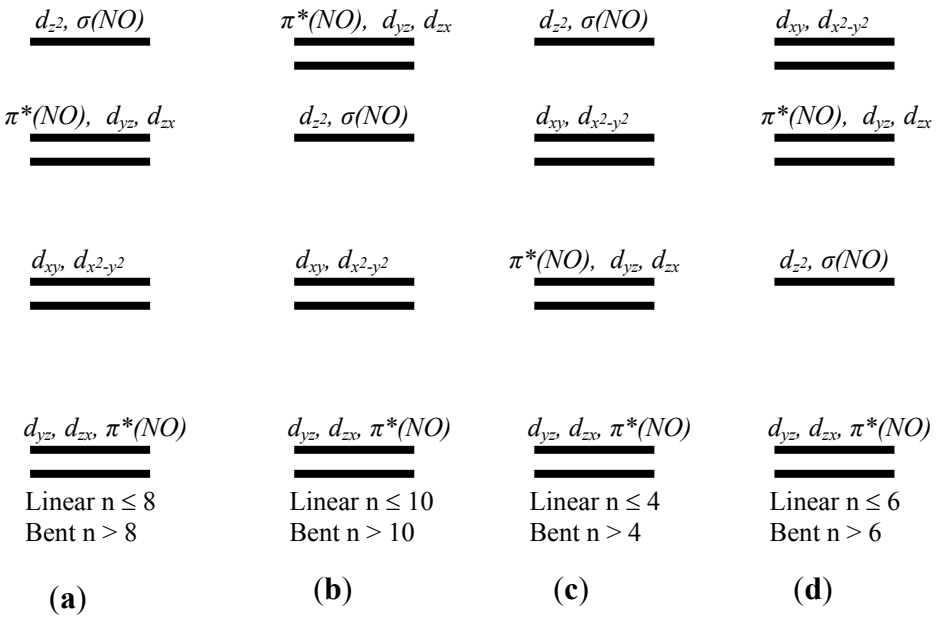

Figure 9. Four possible MO diagrams for the covalent MNO group in $C_{\infty v}$ symmetry. Diagrams a) and b) represent cases where the metal d orbitals of the free ion are higher in energy than the NO π^* orbitals. Diagrams c) and d) represent the cases where the metal d orbitals are of lower energy than the NO π^* orbitals. The influence of *n* on the M-N-O angle is shown for each diagram. Adapted from reference 42.

The coordination of additional ligands to the central metal ion in a complex will lower the symmetry from $C_{\infty v}$ and may have significant effect on the geometry of the MNO unit. A C_{4v} perturbation may, for instance, convert a linear $\{MNO\}^8$ group into a bent $\{MNO\}^8$ group for a molecule from the Figure 9a-category but make a bent $\{MNO\}^6$ into a linear $\{MNO\}^6$ for Figure 9c-category. A relevant example of this perturbation is six-coordinate Heme-NO complexes with an apical NO ligand, where C_{4v} is the maximum symmetry.

In Figure 10, the rightmost diagram illustrates the energy levels of the relevant MNO unit orbitals in a field of C_{4v} symmetry. The bonding combination of the metal d_{z^2} and the NO p_σ – orbital is very low in energy, and mostly localized on the N atom of the NO, thus the lowest orbitals displayed in the diagrams of Figure 10 are the two bonding combinations (with respect to the M and N) of the metal d_{xz}, d_{yz} and the NO π^* orbitals. These orbitals are antibonding with respect to N and O. The metal d_{xy}- orbital interacts with no NO orbital, thus stays localized on the metal and is nonbonding. This would be the case also for the metal $d_{x^2-y^2}$

orbital, but due to the C_{4v} perturbation by the basal ligands, this orbital is significantly elevated in energy compared to for the $C_{\infty v}$ symmetry. Electron configurations which place electrons into antibonding orbitals will cause distortion of the MNO group. If the MO scheme in Figure 10 applies to a six coordinate $\{MNO\}^6$ complex with C_{4v} symmetry, all of the bonding and nonbonding orbitals are filled. Then a $\{MNO\}^7$ complex must place the additional electron in an antibonding orbital, in this case the antibonding combination of the metal d_π and NO π^* orbitals, thus producing a bent MNO unit.

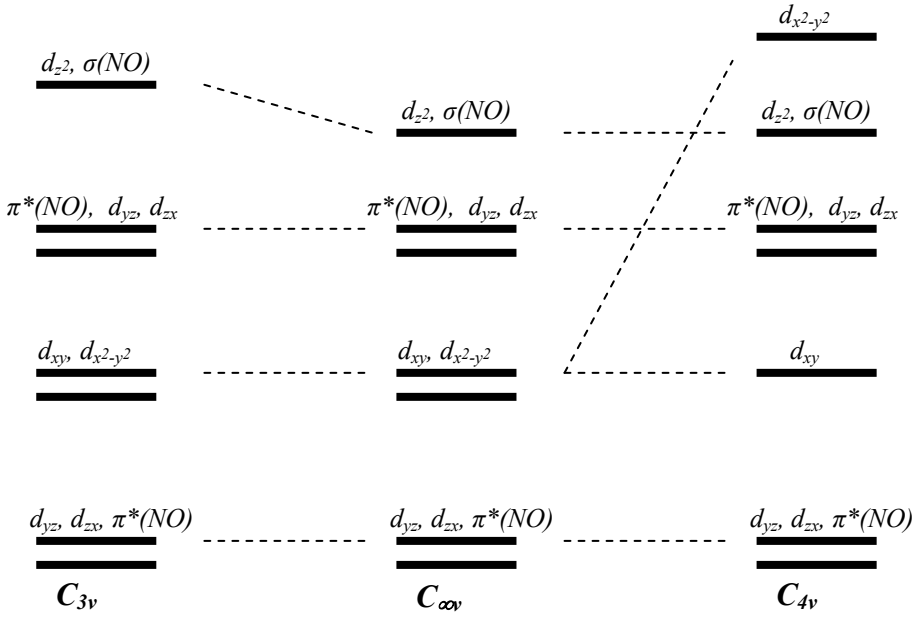

Figure 10. MO diagrams for MNO units in C_{3v} symmetry (left), $C_{\infty v}$ (middle) and C_{4v} (right). Diagrams are modified from reference 39.

Stereochemical Control of Valence

From the above-given discussion we see that transition metal nitrosyl complexes can be usefully discussed as triatomic species being perturbed by the coordination of other ligands to the metal. Thus bonding in mononitrosyl complexes is usefully investigated by examining the perturbations which arise by placing the MNO group in fields of appropriate symmetry.[39]

The physical and chemical properties of the $\{MNO\}^n$ functional group are dictated by:[34, 39]

- The total number of electrons associated with the metal d- and π* NO orbitals.
- The coordination geometry and number about the metal.
- The nature of the occupied one-electron molecular orbitals.

For $n \leq 6$ all $\{MNO\}^n$ groups are linear or nearly so in octahedral geometry (6-coordination). A typical example is $(Por)Mn^{II}(NO)(ImH)$. For $n \geq 7$, $\{MNO\}^n$ groups are bent in octahedral geometry. Typical examples of $n = 7$ and $n = 8$ are $(Por)M^{II}(NO)(ImH)$ where M = Fe, Co respectively. For 5-coordination MNO is linear for $n \leq 6$, $n = 8$ gives linear MNO units in TBP complexes but bent MNO units for SQP complexes. For 4-coordination, $n = 10$ gives a linear MNO unit for tetrahedral coordination geometry about the metal, but a bent MNO unit for planar geometries.

For a given class of complexes additional perturbations can be introduced by changing the metal and/or the donor atoms of the ligands. Because the formal oxidation states of the atoms, the geometries and chemical reactivities of the MNO group are dictated by the overall stereochemistry of the complex ion, Enemark and Feltham introduced the collective term "stereochemical control of valence" for these determining factors.[39] In view of the differences between the electronic structures of linear and bent MNO groups, considerable difference in their chemical reactivity is expected.[34]

Structural Rules for 5-coordinate NO Complexes

In a paper from 1974 Hoffmann and coworkers[43] presented a comprehensive theoretical model of the electronic structure of 5-coordinate nitrosyls. In this paper they discuss the relationship between the SQP geometry with a bent apical nitrosyl ligand and the TBP geometry with a linear equatorial nitrosyl ligand, with the aim of understanding why and how 5-coordinate nitrosyl complexes bend. The answers came in the form of a set of rules (only slightly modified from reference 43):

- The better the σ- or π-donating capabilities of the basal ligands, the more likely is the nitrosyl to bend.
- In compounds of type $ML_2L'_2(NO)$, L trans to L′ having different donor capabilities, the nitrosyl group should bend in the plane containing the poorer donors.
- In a compound of the type ML_2DA, D = π donor trans to A = π acceptor, if the NO group bends in the DMA plane, then it should bend toward the acceptor.
- The nitrosyl is less likely to bend in the equatorial position of a trigonal bipyramid than in the apical site of a square pyramid.

- If a nitrosyl in the equatorial position of a trigonal bipyramid bends, then it would prefer to do so in the axial plane rather than in the equatorial one.
- Nitrosyl groups in axial positions in a trigonal bipyramid and basal sites in a square pyramid prefer to be linearly coordinated.
- In ML_4NO species, if the ligands L are strong π acceptor substituents, a trigonal bipyramid with an equatorial nitrosyl will be preferred. If the ligands L are strong π donors, a range from strongly bent SQP to less bent TBP of geometries is possible.

The arguments go as follows: π donor substituents will raise the energy of the metal d_π and d_σ orbitals (using notation from the $C_{\infty v}$ point group for the MNO unit). The higher the d_σ lies, the stronger its stabilizing interaction with the NO π* in the xz-plane as it bends and the less destabilizing its interactions with NO σ*. If the former dominates, a rising of the energy of the d_σ orbital favors bending. As will raising the xz-plane d_π orbital, by lessen its preference for linear geometry. Thus, the net result of increase in energy of the d_π and d_σ orbitals through donor substitution is to favor bending. Conversely, basal substitution by acceptors lowers the energy of the d_π and d_σ orbitals and by that favoring MNO linearity.

If the four basal donors may be split into two groups L (in the xz plane) and L´ (in the yz plane), the latter being a better donor than the former, then the metal d_π orbitals are no longer degenerate. The better basal donor substituents make the metal a stronger donor in the yz plane, and as the NO bends it loses the weaker π interaction and keeps the stronger one, thus bending in the xz-plane. If two of the four basal ligands are constituted of one good π donor denoted D and one good π acceptor denoted A trans to D, the basal π acceptor orbital mixes into d_π in the DMA-plane (defined as the xz plane for convenience) in a bonding manner and the π donor orbital mixes in an antibonding manner. This gives a secondary node between d_{xz} and the basal donor orbitals, but no corresponding node on the acceptor side. Then if the nitrosyl bends, it will prefer to do so to minimize the antibonding NO σ_2 - d_{xz} interaction, by pointing the NO σ_2 toward the node and preserve the xz-plane NO π* - d_{xz} bonding interaction by pointing the xz-plane NO π* toward the nodeless side. In a linear geometry, the MO of metal d_{z^2} parentage is mostly localized on the metal with only a minor part antibonding NO σ_2 mixed in. As the NO bends, the metal d_{z^2} orbital begins to interact with the xz-plane NO π* orbital. Thus, the NO bond weakens as the π* orbital is populated and the NO group as a

whole gains electron density from the ML_4 fragment. The metal d_π orbitals are degenerate with strong π bonding with the NO π* orbitals in the linear MNO geometry. This interaction is gradually weakened as the NO group bends, and the expected trend is the reverse of the one described for the metal d_{z^2} – NO orbital interaction. The effect set by the metal d_{z^2} orbital dominates because this orbital is closer in energy to the nitrosyl π* orbitals than the metal d_{xz}, thus causing a stronger interaction.[43]

If the metal d_{z^2} orbital is energetically higher than the NO π* orbitals, basal donors that raise the energy of the former would decrease the interaction between the metal d_{z^2} and the NO π* orbitals, since it is now above and thus removed from the latter. The effect is a decreased tendency to bend. The effect of a reversed order of the metal d_{z^2} orbital relative to the NO π* orbitals on M-L charge transfer would be an increased electronic density on the NO because the NO π* orbitals would be populated first. Though, the M-N_{NO} bond is not necessarily weakened because two electrons have switched from an σ* MO to a π* MO.

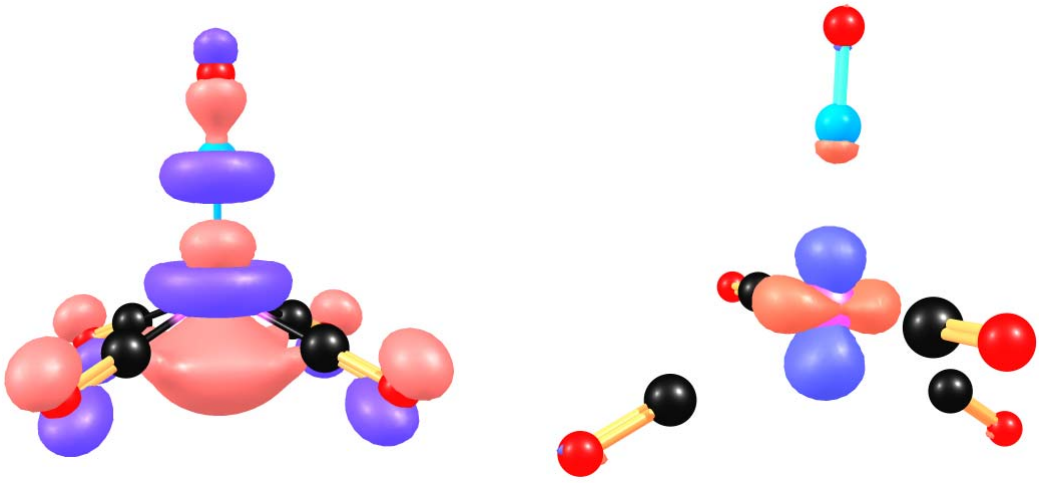

Figure 11. The metal d_{z^2}-NO σ_2 antibonding interaction for the SQP geometry (left) and the TBP geometry (right). For both molecules, the z-axis is along the M-N_{NO} vector and the y-axis is along the face of the paper. The pictured molecules are provided for illustration purposes only.

For both the SQP and TBP geometries, the balance of interactions involving the d_{z^2} orbital, which favor bending, and the d_{xz} and d_{yz} orbitals, which favor linearity, imposes one or the other. The essential difference between the linear NO structure of the SQP and TBP geometries is that for the SQP geometry, the antibonding metal d_{z^2} - NO σ_2 combination (illustrated in Figure 11) cannot be avoided, because the d_{z^2} orbital is the only metal orbital of

a_1 symmetry. For the TBP geometry both d_{z^2} and $d_{x^2-y^2}$ have the same symmetry, and the linear combination $d_{z^2} + d_{x^2-y^2} \sim d_{z^2-y^2}$ (illustrated in Figure 11). This combination takes some electron density from the laboratory z-axis and puts it into the less electronically crowded region along the laboratory y-axis.

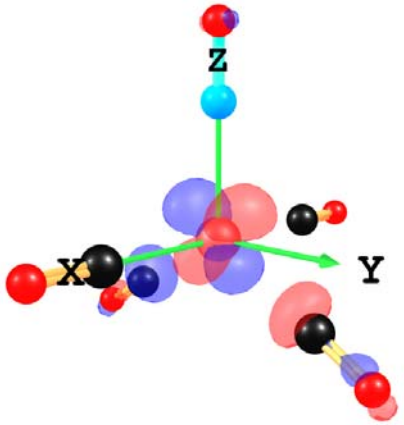

Figure 12. Illustration of the metal d_{yz}-basal ligand orbital σ antibonding interaction. The pictured molecules are provided for illustration purposes only.

The distortion from SQP to TBP causes a characteristic difference between the xz and yz directions by itself, without differential ligand substitution (which would contribute additionally). If the axial positions in the TBP geometry are along the laboratory x-axis, the metal d_{yz} orbitals would be higher in energy than the metal d_{xz} because of σ antibonding character versus the basal ligands (Figure 12). Then the yz plane becomes the better donor plane, and as the nitrosyl bends it should preserve the stronger metal d_{yz} – nitrosyl π* interaction, which implies bending in the xz plane.

5- and 6-coordinate Heme NO Complexes

General Description of MNO Unit Structures in Metalloporphyrin NO Complexes

The metalloporphyrin nitrosyls exhibit distinct MNO bond angles and serve here as an excellent frame of reference for the discussion on low-coordinated NO complexes. For these complexes, which in general have square pyramidal geometries in 5 coordination and pseudoctahedral geometries in 6 coordination, the most important cases are the $\{MNO\}^n$, n = 6-8, being characterized by different M-N-O bond angles of approximately linear for n = 6, lightly bent (140°) for n = 7 and strongly bent (120°) for n = 8. These cases are exemplified

by Fe^{III}-NO porphyrin-, Fe^{II}-NO porphyrin- and Co^{II}-NO porphyrin complexes, respectively.[34, 37, 44]

The MO diagram for a C_{4v} perturbed MNO unit (Figure 10) gives a qualitative explanation for this variation in M-N-O bond angles. For n ≥ 7, because of occupation of MNO antibonding orbitals, the metal d_π in the bending plane changes its bonding character from π to σ due to the bending. Crystallographic studies by Scheidt and coworkers[44, 45] revealed that MNO unit bending was not the only fundamental structural feature of the metalloporphyrin nitrosyls. In addition to the expected bond angles of 144.4° for a $\{MNO\}^7$ system, Ellison and Scheidt[45] reported a tilting of the MNO unit for $\{FeNO\}^7$ porphyrins. An [Fe(OEP)(NO)] complex displayed a metal ion displacement of approximately 0.3 Å above the inner core porphyrin plane (defined by the 4 pyrrole nitrogens, thus termed the N_4 plane) and a 6.5° tilt of the Fe-N_{NO} vector from the N_4 plane normal. Also, the four equatorial Fe-N_{Por} bonds displayed a rather large range of values, pairwise so. The geometrical features reported for this complex were as follows: A MNO unit bond angle of 144.2°, a Fe-N_{NO} distance of 1.722Å and an N-O distance of 1.167Å. In an attempt to reproduce these experimental results, an even greater off perpendicular tilt of 8.2° was found, with the other geometrical key values of 142.7°, 1.731 Å and 1.168 Å, respectively. In a later paper, Scheidt and coworkers[46] confirms the above mentioned findings also for 5-coordinate ferrous porphyrin nitrosyl compounds. A DFT/PW91 study by Wondimagegn and Ghosh[47] assigned this tilting and equatorial asymmetry to molecular orbital interactions.

Wyllie et al.[48] report changes going from five-coordinated to six-coordinated complex for various iron porphyrin NO complexes. Their observations indicate a destabilization of the metal d_{z^2} orbital and thus increasing the MNO unit bending by approximately 5°, the Fe-N_{NO} bond seems somewhat influenced, with an increase of approximately 0.02 Å and decrease of the Fe-N_{NO} off perpendicular tilt by up to as much as 4°.

Electronic Structures in 5- and 6-coordinate Heme-NO Complexes (Paper 1)

We used DFT/PW91 to study electronic and geometric structures of 5- and 6-coordinate heme-NO complexes with the main purpose to study their H-bond acceptor abilities. 5- and 6-coordinate heme-NO active sites were modeled with (Por)Fe(NO) and (Por)Fe(NO)(ImH)

(where Por = porphine and ImH = imidazole).[47] In this study, the heme-NO bonding electronic structure was modeled and some fundamentals of heme-NO bonding were mapped, serving as a later reference for the discussion on low coordinate transition metal nitrosyl and imido complexes.

The optimized geometrical parameters on (Por)Fe(NO) and (Por)Fe(NO)(ImH) are in generally good agreement with experimental metrical parameters on related 5- and 6-coordinate iron porphyrins (See Figure 13).[44, 45, 46]

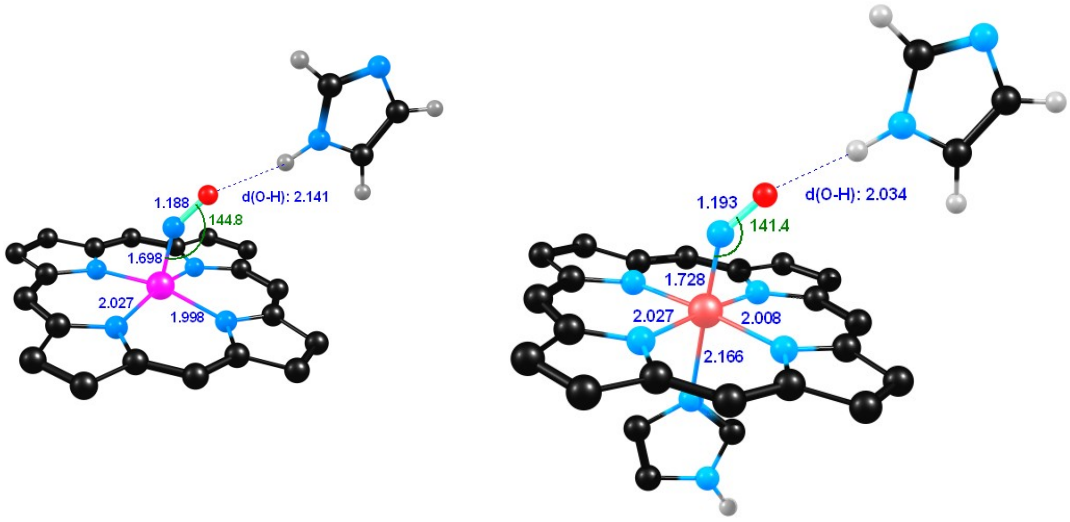

Figure 13. Geometrical parameters of the 5- and 6-coordinate complexes investigated in Paper 1.

The Fe-N_{ImH} distance is rather long, reflecting the antibonding metal (d_{z^2}) – (ImH) trans ligand interaction present in the SOMO of (Por)Fe(ImH)(NO) (Figure 14). The Fe-N_{NO} vector is tilted relative to the N_4-plane normal, which has also been observed experimentally.[44, 45, 46] The direction of the tilting is explained largely by the *a´* Fe(d_π)-NO (π^*) $\pi \rightarrow \sigma$ interaction and the tilting of the metal d_{z^2} ligand the opposite way, which contributes to reduce the metal d_{z^2} - NO σ_2 antibonding interaction.

With respect to the hydrogen bond abilities, we found hydrogen bonding present for both 5-coordinated and 6-coordinated heme-NO models, both resulting in a small increase in the NO-distance. In general, our findings suggest that distal hydrogen bonding has little effect on the energetics of the dorsal Fe-His linkage (later confirmed by Spiro and coworkers[49]).

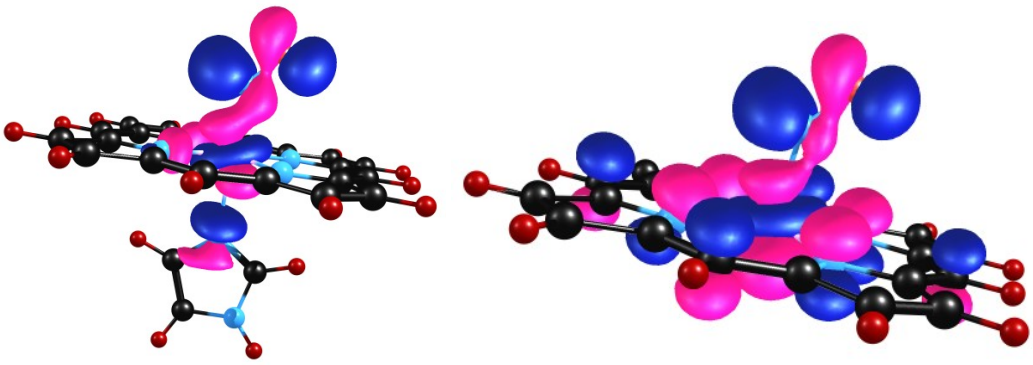

Figure 14. The 6-coordinate (left) and 5-coordinate (right) SOMOs for the heme-NO system investigated in Paper 1.

5-coordinate Terminal Transition Metal Nitrosyls

Nonheme $\{MNO\}^6$ Complexes

Mn(NO)(5,5-TC), a $\{MnNO\}^6$ complex reported by Franz and Lippard,[50] displayed a metal centre with idealized TBP coordination geometry with the nitrosyl in an equatorial position. For this complex, the M-N-O angle was nearly linear (174.1°) and also the bond distances were within expectations, 1.699 Å for the Mn-N_{NO} distance and 1.179 Å for the N-O distance, respectively. From spectroscopic characterization, this complex was assigned a quintet spin state, a $[Mn^{III}NO^{-}]^{2+}$ complex.

For a complex also in TBP geometry, though with the NO ligand in an axial position, Conradie et al.[51] reported a similar MNO unit structure (Figure 15). This complex, $[Fe(NO)(PS3^*)]^{-}$, characterized both with spectroscopic and computational methods showing a S = 1 spin state, displayed an almost linear M-N-O bond (175.2°) from X-ray crystal structure, a M-N_{NO} distance of 1.676 Å and a N-O distance of 1.154 Å.

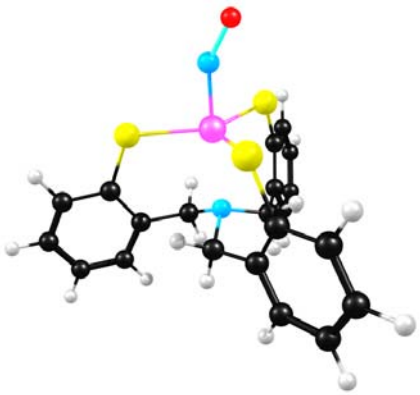

Figure 15. The $[Fe(NO)(PS3^*)]^{-}$ structure investigated by Conradie et al.[51]

Nonheme $\{MNO\}^7$ Complexes

In contrast to expectations that stem from knowledge about heme complexes[39] a nonheme $\{MNO\}^7$ complex with an essentially linear MNO unit was been reported by Franz and Lippard.[52] The Fe(NO)(5,5-TC) complex has a central metal in idealized TBP coordination geometry with the NO group in the equatorial position (TBP_{eq}). The geometrical features for this complex are all within the range of values reported for the $\{MNO\}^6$ complexes above; The M-N-O bond angle was found to be 174.3°, the $M\text{-}N_{NO}$ distance 1.670 Å and the N-O distance 1.176 Å. From this stems the assumption by Lippard and coworkers[50, 52] of similar electronic states for the NO group for both the $\{MNO\}^6$ and $\{MNO\}^7$ tropocoronand complexes. The overall molecular spin for the iron-nitrosyl tropocoronand was by spectroscopic methods identified to arise from Fe^{III} S = 1/2 antiferromagnetically coupled to S = 1 NO^-.

In a computational paper from our group, Conradie and Ghosh[53] attempt to explain a linear $\{MNO\}^7$ unit for the SQP geometry of the $[Fe(NO)(CN)_4]^{2-}$ complex. This low-spin molecule displays an exact linear M-N-O angle, and the SQP C_{4V} point group structure was preferred by 0.78 eV over the alternative TBP structure. The reported additional geometrical features from the computational study of this molecule were a $M\text{-}N_{NO}$ distance of 1.66 Å and a N-O distance of 1.19 Å.

In a joint experimental and computational paper, Conradie et al.[51] reported a S = 3/2 spin state $\{FeNO\}^7$ complex with a TBP coordination geometry about the metal ion and displaying M-N-O angles of 145.9° and 147.8°, corresponding N-O distances of 1.18 Å and 1.11 Å from X-ray crystal structure analysis. The $M\text{-}N_{NO}$ distance for this $[Fe(NO)NS3)]^-$ compound was 1.756 Å, quite a bit long compared to the one in Fe(NO)(TC-5,5). By the authors, the key determinant of the FeNO bent geometry was assigned to the antibonding d_{z^2} interaction, destabilized by the trans amine ligand lone pair electrons. This assumption was supported by comparison with a non-trans ligated complex.[51]

In an attempt to draw parallels between heme and nonheme nitrosyl systems, Patra et al.[54] reported a $\{FeNO\}^7$ complex with essentially square pyramidal coordination geometry around the central iron, displaying a typically bent Fe-N-O angle of 144.7°. The low-spin state of this

complex was by the authors from analysis of the X-ray geometry assigned to comprise an intermediate spin Fe^{III} antiferromagnetically coupled to a triplet spin NO^-. This is in line with what is reported also for the Fe(NO)(5,5-TC) complex.[52]

Table 3. Concluding the geometrical features reported for 5-coordinate nonheme transition metal complexes with terminal nitrosyl ligands.

Complex	Coord. Geom.	Spin	M-N_{NO} (Å)	N-O (Å)	∠ MNO (°)	Ref
[(bpb)Fe(NO)]	SQP	1/2	1.713	1.182	144.7	54
Fe(NO)(5,5-TC)	TBP_{eq}	1/2	1.670	1.176	174.3	52
$[Fe(NO)NS3)]^-$	TBP_{ax}	3/2	1.756	1.11 1.18	145.9 147.8	51
$[Fe(NO)(CN)_4]^{2-}$	SQP	1/2	1.66	1.19	180	53

A Linear $\{FeNO\}^7$ Low-spin Unit (Paper 2)

With DFT/PW91 we investigated the electronic and geometrical structure of the Fe(*5,5*-TC)NO complex and the corresponding simplified models Fe(tam)NO and Fe(me_2tam)NO (see Figure 16). The Fe(*5,5*-TC)NO has previously been characterized by spectroscopic methods,[52] but our study provides an additional MO description of the complex.

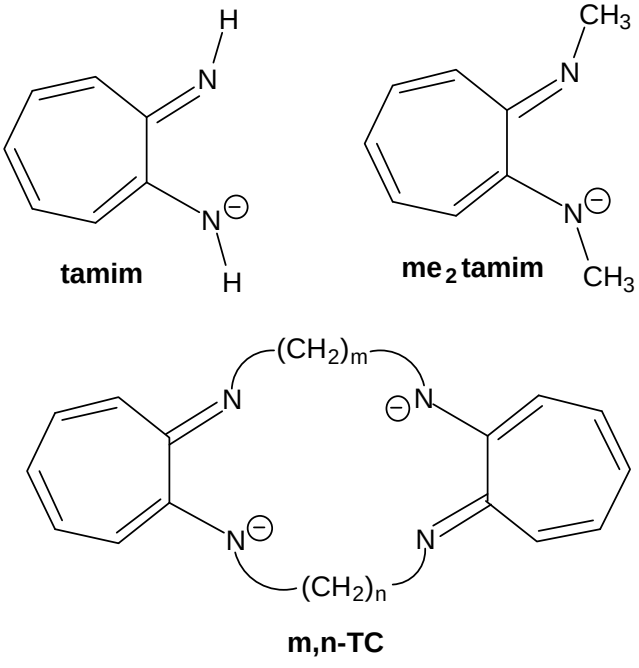

Figure 16. The tamim (tam), me_2tamim (me_2tam) and tropocoronand ligands, $[m,n\text{-}TC]^{2-}$ investigated in Paper 2.

$\{FeNO\}^7$ S = 1/2 and S = 3/2 systems with all three ligands were optimized. We investigated possible geometries of the complex by applying starting geometries defined as SQP, TBP with the NO-group in the axial position (TBP_{ax}) and TBP with the NO-group in the equatorial position (TBP_{eq}) (see Figure 17) by applying symmetry constraints to the input. The *S* = 1/2 spin state was favored for all of the molecules studied, consistent with experiment,[52] by a substantial margin. Thus we did not include the S = 3/2 states in the overall discussion.

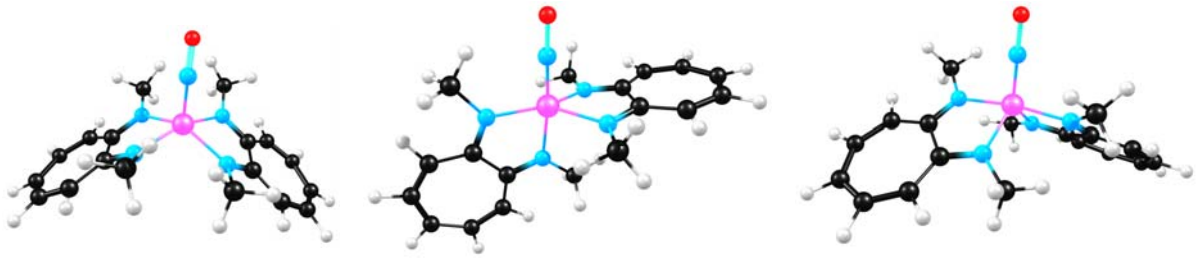

Figure 17. The SQP geometry (left), TBP_{ax} geometry (middle) and TBP_{eq} geometry (right).

For $Fe(tam)_2NO$, the lowest-energy conformation corresponds to SQP coordination geometry, with the TBP_{eq} geometry only about 0.1 eV higher in energy. For the $Fe(me_2tam)_2NO$, this is reversed and the split is slightly larger. For both, the TBP_{ax} geometry is significantly higher in energy. The results for Fe(*5,5*-TC)NO are qualitatively similar to those for $Fe(me_2tam)_2NO$; the TBP_{eq} geometry has the lowest energy, the SQP geometry is nearly 0.9 eV higher in energy, and the TBP_{ax} form is higher still. The reversal of stereochemical preference between $Fe(tam)_2NO$, on the one hand, and $Fe(me_2tam)_2NO$ and Fe(*5,5*-TC)NO, on the other hand, basically indicates that alkylation of the tamim ligands, whether with methyl groups or with the polymethylene tethers of the *5,5*-TC ligand, tips the stereochemical preference from SQP to TBP_{eq}.

For the SQP and TBP_{eq} geometries, none of the higher occupied MOs exhibits significant metal-ligand antibonding interactions, whereas the SOMO as well as the majority spin $HOMO^{-2}$ and minority spin $HOMO^{-1}$ in the TBP_{ax} case all exhibit significant metal-tamim σ antibonding character (shown in Figure 18). Also, MO investigations indicate that the metal-tamim bonding interactions are stronger for the SQP and TBP_{eq} geometries than for the TBP_{ax} geometry; a strong low-lying metal-tamim bonding interaction in the majority-spin $HOMO^{-19}$ for the SQP and TBP_{eq} cases has no analogue for the TBP_{ax}.

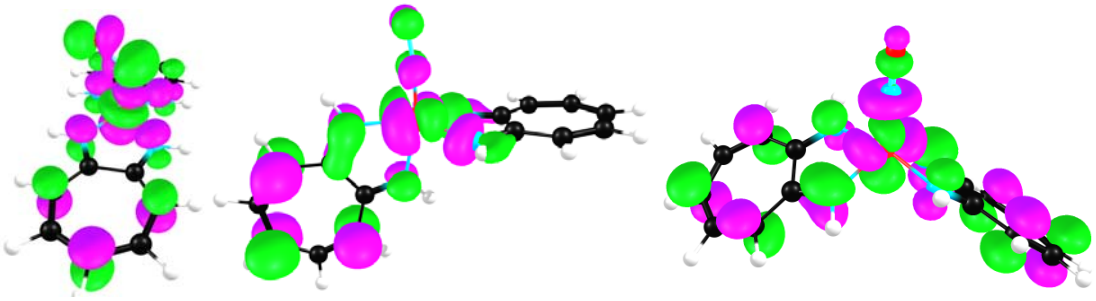

Figure 18. The majority spin HOMOs (SOMOs) of the investigated tamim complexes.

For the TBP_{eq} geometry of $Fe(tam)_2NO$ and Fe(*5,5*-TC), the electronic configuration of the metal may be described as $(d_{xz}, d_{yz})^4 d_{xy}^2 d_{x^2-z^2}^1$ and the majority-spin HOMO^{-2} may be viewed as Fe d_{xy}-based. The SOMO is best described as a $d_{x^2-z^2}$ orbital rather than primarily d_{z^2}. This may also be seen from the spin-density profile, which is consistent with the spectroscopic characterization of the $\{FeNO\}^7$ center in Fe(*5,5*-TC)NO as a Fe^{III} ion antiferromagnetically coupled to a NO^- group.[52]

DFT geometry optimization reproduces the experimentally observed conformation for the Fe(*5,5*-TC)NO molecule.[52] Two of the three equatorial Fe-N vectors in the TBP_{ax} structures are > 2.00 Å, longer than all other Fe-N distances in this study, and these two distances reflect the metal-tamim antibonding interactions in the SOMO of all of the TBP_{ax} species.

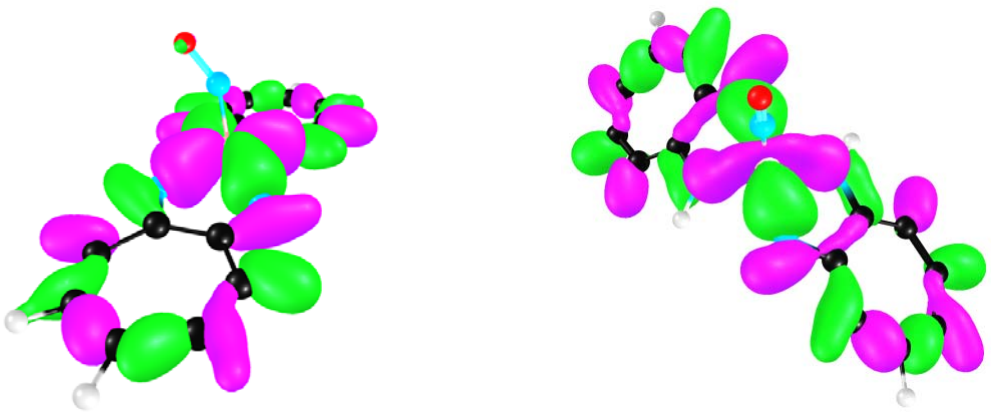

Figure 19: The low-lying metal-tamim bonding interaction for the SQP (left) and TBP_{eq} (right) geometries.

As expected for low-spin Fe^{III} centers, the other Fe-N distances involving the tamim fragments are relatively short: 1.91-1.95 Å for SQP $Fe(tam)_2NO$, 1.93-1.94 Å for TBP_{eq}

$Fe(tam)_2NO$, and 1.95-1.98 Å for TBP_{eq} Fe(*5,5*-TC)NO. The calculated Fe-N_{NO} distances are considerably shorter in the TBP_{eq} structures than in the SQP ones. For the TBP_{eq} and for the full FeTC-complex, they are approximately the same (1.66 versus 1.65) and in range with the experimentally reported distance of 1.67 Å.

To find out why the FeNO unit is bent in the SQP structures and almost linear for TBP_{eq} conformations, the MO energies for Fe(*5,5*-TC)(NO) (having TBP_{eq} coordination geometry) were plotted as a function of the Fe-N-O angle in a Walsh type diagram.[55] These studies indicated that while the Fe-N-O angle favors Fe-N-O σ bonding (lowers the energy of the d_{z^2} or $d_{x^2-z^2}$-based MO), it raises the energies for Fe(d_π)-NO(π*) bonding interaction MOs. As a result the net energetic cost of FeNO deformation is small. Thus, a TBP_{eq} Fe(*5,5*-TC)(NO) structure with an Fe-N-O angle constrained to 140°, but otherwise fully optimized, is only about 0.1 eV higher than the global minimum with a near linear FeNO unit. For the TBP Fe(*5,5*-TC)(NO), the SOMO is Fe $d_{x^2-z^2}$ in character, with the Fe-N_{NO} vector along the laboratory z-axis, and this d orbital is σ-antibonding with respect to NO. Thus π-bonding dominates the Fe-NO interaction, leading to an essentially linear FeNO unit and a short Fe-N_{NO} distance, for this complex.

Nonheme $\{MNO\}^8$ Complexes

Five coordinate complexes containing the $\{CoNO\}^8$ group exhibit Co-N-O angles ranging from 120°-180°.[56] For TBP geometries, the dominating {CoNO} unit bond structure is linear, as opposed to the strongly bent domination for {CoNO} units in SQP geometries. For $Co(NO)L_4$ the maximum symmetry possible is C_{4v}, and the metal (d_{z^2}) parentage MO can be above or below the (d_{xz}, d_{yz}, π*) parentage antibonding orbitals for these complexes (Figure 9 and Figure 20).

With the (d_{z^2}) orbital above the (d_{xz}, d_{yz}, π*) antibonding orbitals, we can see from Figure 20 that the totally antibonding (d_{xz}, d_{yz}, π*) orbitals will be doubly occupied. Then the $\{CoNO\}^8$ group will bend producing a $Co(NO)L_4$ molecule in C_s symmetry. If the order is reversed, the two additional electrons will be put in the d_{z^2} parentage MO and the $\{CoNO\}^8$ group will not bend, but the $Co(NO)L_4$ complex distorts to TBP_{eq} geometry in C_{2v} symmetry. This

distortion makes the d_{z^2} parentage MO less antibonding, by easing the metal d_{z^2} - NO σ* antibonding interaction, and thereby lowering the energy of the complex. Thus for five coordinate complexes of the $\{CoNO\}^8$ group, the choice between a TBP structure of C_{2v} symmetry and a SQP structure of C_{4v} symmetry is dictated by the relative energies of the d_{z^2} – and (d_{xz}, d_{yz}, π*) parentage orbitals of the hypothetical C_{4v} linear species.

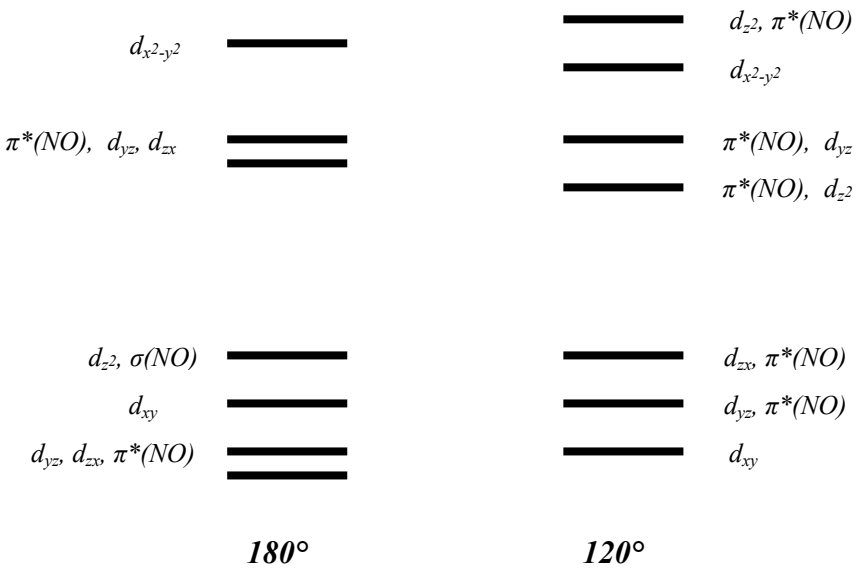

Figure 20. Arrangement of molecular orbitals in five-coordinate $\{MNO\}^n$ when M-N-O is 180° (left) and 120° (right).

Interestingly, Lippard and coworkers[57] reported both a SQP and a TBP geometrical $\{CoNO\}^8$ with essentially bent MNO units. A [(Co(NO)(TC-3,3)] was claimed to be paramagnetic, had a SQP coordination geometry and displayed an essentially bent M-N-O bond of 127.3°. A [(Co(NO)(TC-4,4)] was in contrast claimed to be diamagnetic, had a TBP coordination geometry and displayed Co-N-O bond angles of 128.9° and 134.9° from X-ray crystallography.

4-coordinate Terminal Transition Metal Nitrosyls

Only very few 4-coordinate first-row transition metal complexes with a terminal NO ligand have been reported. An $\{FeNO\}^7$ complex, $[Fe(StBu)_3(NO)]^-$, reported by Harrop et al.[58] has a Fe-N_{NO} distance of 1.711 Å, a N-O distance of 1.168 Å and a Fe-N-O bond angle of 174.2°. By spectroscopic examinations, this complex is assigned to be an S = 5/2 Fe^{III} ion antiferromagnetically coupled to an S = 1 NO^-, giving an overall S = 2 state. The metal ion

coordination geometry in this complex is best described as a pseudotetrahedral arrangement with the NO in an apical position. This is clearly in line with the conclusions made by Enemark and Feltham.[39] DFT results reported by Conradie et al.[59] displayed comparable geometrical features, with a Fe-N_{NO} distance of 1.681 Å, an N-O distance of 1.202 Å, a Fe-N-O bond angle of 178.5° and also confirming the spin state assignment by Harrop et al.[58]

4.2 Low Coordinate Imido Complexes

Introduction to Imido Ligands

The imido group is a derivative of amines, NR^{2-} and isoelectronic with O^{2-}. Though, the imido ligand in contrast to the oxo ligand may be either linear or bent.

Figure 21. The linear (left) and bent (right) bonding arrangement of terminal imido ligands.

The R-groups can be H, alkyl, aryl, tosyl or other organic groups. Imido compounds are commonly found in transition metal complexes with oxidation states ≥ 3. The imido group's high capacity for electron donation acts to stabilize high oxidation states. Imido ligands are also referred to as imides or nitrenes, and a transition metal imido unit has the general formula M = NR where there is a double bond between the metal center and the nitrogen atom.[34] In addition, the lone pair on nitrogen usually donates to the metal center as well, providing a three-bond interaction with the metal. The terminal MNR ligands are usually relatively linear (∠MNR of 170-180°).

In general, working with transition metal complexes, the imido unit is considered to be doubly negatively charged, whereas those that work with low-valent complexes tend to consider it a neutral ligand.[60] Thus, when specifying how many electrons an imido ligand donates it is therefore necessary to state which electron counting formalism is being used and to consider whether the nitrogen lone pair is participating in the bonding or not. Imido ligands are good π donors and the M-N-R bond angle can be considered as an indicator of the degree of π donation from nitrogen (see Table 4).

Table 4. Summarizing the bonding modes of terminal imido ligands. Modified from Toraki.[60]

Unit geometry	Linear metal-imido	Bent metal-imido
Hybridization of nitrogen	sp	sp^2
Idealized bond angle	180°	120°
Electron donation NR^{2-}	6 e^-	4 e^-
Electron donation neutral	4 e^-	2 e^-

In general, the only circumstances under which imido ligands are not linear: [60]

- If there is no empty d-orbital on the metal that has the proper symmetry to overlap with the nitrogen lone pair (sp) orbital.
- If the metal electron count is already 18 electrons in which case it will usually have another imido ligand which is linear.
- If the imido ligand is part of a cyclic or multidentate ligand which physically constrains it from being linear.

In tending to maintain an 18e^- count in electron rich compounds, and depending upon the nature of the ancillary ligands, bending may occur as required.

Metal-Ligand Multiple Bonds

Transition metal compounds, such as vanadyl oxo-, uranyl oxo- and permanganate- and osmium tetroxide complexes all display M = O bond distance in the range of 1.59-1.66 Å, indicating multiple bonding. The π component in these bonds is regarded as arising from oxo π → metal d_π electron flow. Since this is the opposite of electron flow in π-bonding ligands of the CO type, it is not surprising that the latter are the more stable in low oxidation states and the oxo ligands more likely to stabilize high oxidation states. The M = O bonding is typically affected by the nature of group trans to it, giving the oxo ligand a strong trans influence. Donors that increase electron density on the metal tend to reduce its acceptor properties, thus lowering the M-O multiple bond character. Because of the strong trans influence, ligands trans to oxygen may be labile.[34] In contrast to metal-oxo compounds, compounds containing metal-imido linkages are often better represented by M≡NR,[3] and in most cases something in between a double and a triple bond. There are actually few cases where the presence of a long M-N bond (≥1.8 Å) and a distinctly non-linear arrangement (∠ M-N-R ≤ 160°) are found. For most cases, the distances are ~1.7 Å and the angles > 170°, especially when the arrangement

of the other ligands about the metal is symmetrical enough to allow for two metal d_π – imido π interactions of equal importance.[34] Simple electron counting using the Effective Atomic Number Rule (EAN, 18 electron rule) provides a useful method of classification of organoimido complexes. The maximum electron count (MEC) is defined as the electron count which is calculated if all amphoteric ligands donate the maximum possible number of electrons to the metal.[61]

Introduction to Transition Metal Complexes with Terminal Imido Ligands

In a review on transition metal imido complexes dating back to 1980, Nugent and Haymore commented on the paucity of first-row transition metal complexes containing multiple bonded ligands.[61] At that time most of the organoimido complexes reported contained 2nd and 3rd row transition metals. Generally, this picture is now somewhat altered.[3]

Because of the strong π bonding capabilities of the imido ligand (NR^{2-}), it is naturally compared with the isoelectronic (by EAN rule) nitrido- (N^{3-}) and oxo (O^{2-}) ligands which share this property. A comparison of the oxo and organoimido ligands in the 1980 review in similar coordination environments showed that the M = O distances are about 0.05 Å shorter than the corresponding M = NR distances. This suggests that the M = NR bond is weaker than the corresponding M = O bond. Also, one might have assumed that the trans influence of organoimido ligands should be appreciable owing to the short metal-nitrogen distances. This picture, though, is complicated. For six coordinated MEC 18 electron complexes, there is no significant sign of trans influence.

Of the 12 terminal second- and third-row transition metal mono-imido complexes reported in the 1980 review, only 3 display an M-N-R bond angle of less than 170°. The short metal-nitrogen distances in organoimido complexes seem to vary over a large range from 1.61 - 1.79 Å, and this variation can be rationalized on the basis of (1) the size of the metal (2) the coordination number about the metal ion and (3) the MEC. All complexes with MECs of 18 or less should have metal-nitrogen triple bonds. The reactivity of the terminal imido ligand in transition metal complexes depends on the following factors: (1) The transition metal, (2) the d-electron count of the metal ion (e.g. oxidation state), (3) the ancillary ligands, which dictate

the spin state. All factors contribute to the π interaction between the ligand p-orbitals and the metal d-orbitals. As a simplification of this interaction, one extreme would be when the π* orbital is mostly metal d in character (case A) and the other when the π* orbital is mostly ligand p in character (case B). In case A the metal is considered to be electrophilic and hence a nucleophilic ligand is expected to result. For case B this is reversed, the ligand is predicted to be electrophilic when the π* orbital is mostly ligand in character. Thus typically expected for early transition metal complexes is nucleophilic behavior of the ligand in high oxidation states and for late transition metals is electrophilic behavior in low oxidation states.[62] Therefore, as one moves up and to the right in the periodic table for transition metals, the amount of ligand character to the π* orbital increases and the electrophilicity of the ligand increases.[3]

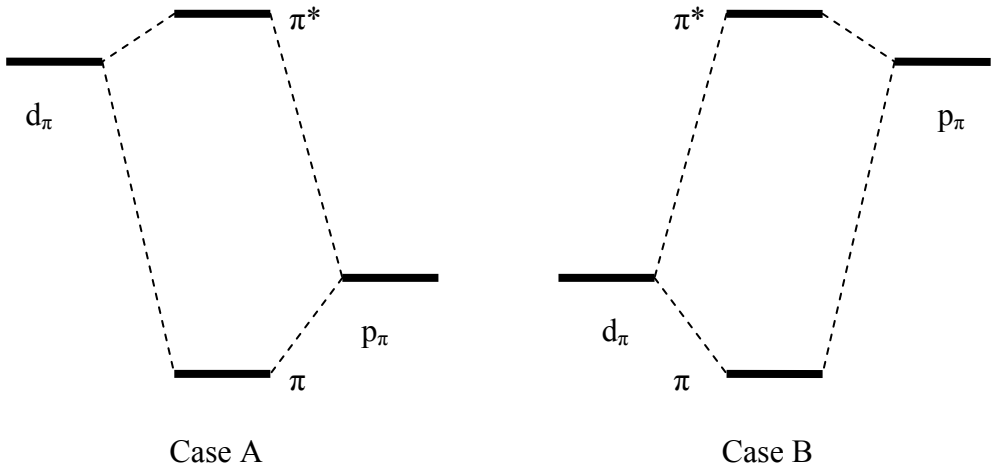

Figure 22. Case A represents a nucleophilic ligand and Case B represents an electrophilic ligand. Adapted from Eikey et al.[62]

3-coordinate Trigonal-Planar Imido Complexes

Reports on three-coordinate transition metal complexes with terminal imido ligands are sparse and rather recent. Warren and his group have reported one d^6 Co^{III}-imido[63] and one d^7 Ni^{III}-imido[64] compound, both displaying a trigonal planar geometry with moderately bent M-N-C bond angles of 161.5° and 164.5° in the plane of the basal ligands, respectively. For both the M-N_{Im} distances were in the range of 1.64-1.66 Å.

Additionally reported DFT results for the d^6 complex supported the presence of a low-spin complex stabilized by σ and π donations from the imido ligand to the metal, leading to

considerable multi bond character in the metal-imido unit in this 16 electron (EAN) three coordinate complex.[63] For the Nickel d^7 complex the additional electron typically would be in a metal d_π - imido p_π antibonding orbital, and alternatively the complex may be described as a Ni^{II} cation stabilized by an imidyl ($RN^{\bullet -}$) radical. This latter description was supported by reactivity analysis.[64]

Eckert et al.[65] presented a three coordinated iron-imido species characterized by spectroscopy, but they did not present a structure due to the instability of the complex. Supportive DFT-calculations assigned this species to be a quartet spin (S = 3/2) Fe^{III} imido complex with a Fe-N_{Im} bond distance of 1.68 Å and a rather linear Fe-N-C vector.[65] This complex, going from three- to four-coordinate, establishes pseudotretrahedral coordination geometry about the metal and thus reduces the splitting of the orbitals by the ligand field. Hence a sextet ground state. As a result of population of the second π* orbital in the 4-coordinate sextet state, the Fe-N bond length is prolonged from 1.68 Å to 1.74 Å. Binding of pyridine (the fourth ligand) also causes substantial bending of the imido ligand (∠ Fe-N-C of 155.1°) and the nitrogen atom has much more spin density in the four-coordinate complex (0.82 e^-) than in the three-coordinate (0.23 e^-). The calculations suggests that the ligand induced change in reactivity going from three-coordinate to four-coordinate is accompanied by (1) a weaker ligand field at iron, (2) a weaker (longer) Fe-N_{Im} bond and a more bent Fe-N-C angle, (3) a possible spin-state change that leads to enhanced radical reactivity at the imido nitrogen. [65]

DFT results from our group on a series of three coordinated first-row M^{III} (including Fe^{IV}) imido complexes displayed essentially linear M-N-C bonds (in the range of 176.6º-179.6º) and M-N_{Im} distances in the range of 1.657 Å (for Fe^{IV}) to 1.762Å (for Cu^{III}).[66] Conradie and Ghosh[66] noted an unexpected stability of the metal d_σ orbital.

4-coordinate First-row Transition Metal Terminal Imides

Pseudotetrahedral Complexes with Linear or Near Linear M-N-R Bond Vector

The first structural characterization[3] of a terminal iron-imido linkage describing a pseudotetrahedral Fe^{IV}-imido complex with an M-N-C bond angle of 178.6º and a Fe-N_{Im}

distance of 1.635 Å, was reported by Verma et al.[67] A tris(phosphino)borate ligated Fe^{IV}-imido complex[68] confirms the findings reported by Verma et al.[67] for d^4 metal-imido complexes, displaying a Fe-N_{Im} distance of 1.634 Å and a Fe-N-R bond angle of 176.2º. Spectroscopic methods indicate this complex to be a spin triplet (S = 1), which is in agreement with the orbital picture diagram suggested by the authors (Figure 23) $(d_{z^2})^2(d_{xy})^1(d_{x^2-y^2})^1(d_{xz})^0(d_{yz})^0$. For the corresponding hypothetical Mn^{III}-imido complex, DFT/B3LYP results reported by Lu et al.[69] predicts a triplet ground state, displaying a Mn-N-R bond angle of 179º and P-Mn-P (from basal ligands) bond angles of between 90-92°. For d^5 iron–imido complexes in pseudotetrahedral geometry, the Fe-N_{Im} distances are in the range of 1.63-1.66 Å and Fe-N-R bond angles in the range of 170-177º.[68, 70, 71, 72] Spectroscopic methods assigns the unpaired electron in these complexes to a nonbonding orbital orthogonal to the metal-imido vector.[68, 70]

The class of d^6 imido complexes will be constituted of Fe^{II} and Co^{III} complexes, showing the same range of geometrical values as the d^4 and d^5 classes.[3] These spin singlet complexes have metal-imido bond angles between 170-180º and metal-imido distances of 1.64-1.66 Å.[71, 72, 73, 74] DFT/B3LYP investigations accompanying the spectroscopic results from the Peters group[71] propose the following electronic structure for these S = 0 compounds: $(d_{z^2})^2(d_{xy})^2(d_{x^2-y^2})^2(d_{xz})^0(d_{yz})^0$, this corresponds to $(a_1)^2 + (e)^4$ in C_{3v} point group notation.

Hu et al.[75] reported a TBP d^6 Co^{III} imido species with a Co-N_{Im} bond within the proximity (1.675 Å) of the other reported Co-N bond distances and a Co-N-C bond angle of 168.2°, which, together with the short metal-imido bond, is indicative of a strong multiple bond character within the Co-N_{Ar} entity. The N_{Im}-C_{Ar} distance of 1.386 Å is significantly smaller than that of an N–C single bond (1.47 Å),[76] suggesting also a substantial degree of electron delocalization within the imido-aryl ligand unit. DFT calculations supporting the experimental results showed an orbital splitting diagram for Co^{III} adopting a $(d_{xy})^2(d_{x^2-y^2})^2(d_{z^2})^2(d_{xz})^0(d_{yz})^0$ singlet state, as expected. The MOs of metal d_{xz} and d_{yz} origin are greatly destabilized by strong π antibonding interaction with the imido π lone pairs and thus lie at highest energies, and the six d-electrons occupy MOs up to the d_{z^2} orbital, which is σ antibonding with respect to the Co-NR bond. Although the metal-imido group was often formulated as a triple bond,[3] simple MO arguments describes the bonding within the cobalt imido unit reported by Hu et

al.[75] as a formal double bond. When the antibonding metal d_{z^2}-imido σ orbital is occupied, the bond between the metal and the imido group has no σ contribution, thus being a double bond with only π contribution.

To elaborate the experimental results on metal-imido compounds, Wasbotten and Ghosh reported a DFT study on three different classes of tripodal supporting ligands, namely the trisphosphine-, the tris(N-heterocyclic)carbene- and the hydrotris(pyrazolyl)borate class of ligands.[77] Wasbotten and Ghosh found that the tripodal supporting ligand played a significant role in tuning the spin state energetics for pseudotetrahedral d^6 cobalt-imido complexes. This work also provided theoretical structural data on d^3, d^4 and d^5 transition metal imido complexes in pseudotetrahedral geometries. The d^3 Cr^{III}-imido complex was assigned as S = 3/2 $(d_\delta)^1(d_{\delta'})^1(d_\sigma)^1$ for both the trisphosphine- (mebp3) and the hydrotris(pyrazolyl)borate (Tp) class of ligands. For the Mn^{III} (d^4) complexes, calculations indicated that the triphosphine Mn^{III}(NMe) would display an S = 1 ground state while the hydrotrispyrazolyl $Mn^{III}(N^tBu)$ would yield a high-spin S = 2 species. Correspondingly, for the Fe^{III} (d^5) complexes calculations indicated that the Fe^{III}(mebp3)(NMe) would display an S = 1/2 ground state with a slightly bent Fe-N-R bond vector while the $Fe^{III}(Tp^{tBu,Me})(N^tBu)$ would yield a high-spin S = 5/2 species with a perfectly linear Fe-N-R vector. Thus switch between the hydrotrispyrazolyl and triphosphine basal ligands completely reverse the spin state energetics. The hydrotrispyrazolyl $M^{III}(N^tBu)$ high-spin species for both Fe and Mn displayed quite long optimized M-N_{Im} distances (1.778 Å and 1.787 Å, respectively).

As seen above, all experimentally reported d^4, d^5 and d^6 pseudotetrahedrally coordinated mononuclear, terminal metal-imido compounds display relatively short metal-imido distances (≤ 1.66Å) and relatively linear metal-imido bond angles (≥ 170º). These observations are consistent with strong π-interaction between the metal and the imido group. The presence of two strong π-bonds from the imido linkage together with the strong field executed by the tris(phosphino)borate ligands affords a low-spin ground state in both Fe^{II} and Fe^{III} systems, despite their low coordinate geometries.[3] DFT investigations indicate that these species are best described by a two over three d-orbital splitting diagram[71] in which an orbital of metal d_{z^2} parentage lies at low energy, close to the metal d_{xy} and $d_{x^2-y^2}$ parentage orbitals (see Figure 23).

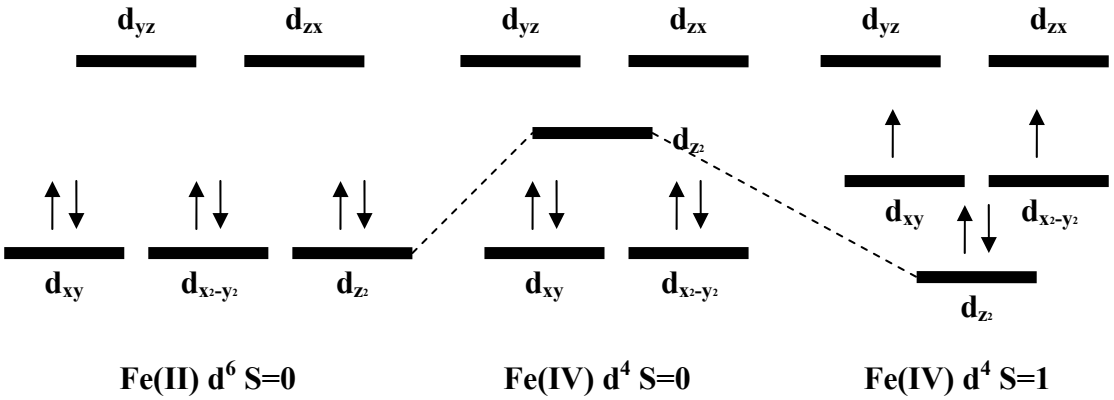

Figure 23. Qualitative MO diagrams for terminal imide (Fe^{II}) and nitride (Fe^{IV}) complexes of three fold symmetry (pseudotetrahedral geometries). Adapted from Mehn and Peters.[3]

Electronic Structure of Pseudotetrahedral Iron-Imido Complexes (Paper 4)

Using DFT/PW91, we have investigated the electronic structure of $Fe^{III/IV}$-imido complexes with the phosphineborate supporting ligands with a local C_{3v} coordination about the metal. The primary aim of this study was to understand the stability of the metal (d_σ)-N_{Im} (p_σ) antibonding orbital relative to the metal d_π-orbitals. Fe^{III} imido, Fe^{IV} imido and Fe^{IV} nitride complexes were investigated using essentially two different ligand systems (see Figure 24).

Our calculations confirm $d_\delta^2 d_{\delta'}^2 d_\sigma^1$ electronic configurations for Fe^{III}-imido complexes of this type. However, geometry optimization of a sterically unencumbered model complex indicated a bent (162°) imido linkage. This is contradictory to the linear imido groups presented for the sterically hindered complexes that have been studied experimentally.[68] Under C_{3v} symmetry constraint, the Fe^{III}-imido molecular orbital energy-level diagram indicates the existence of near-degenerate $^2A_1$ and ^2E states, and the bending of the imido group appears to be ascribable to a pseudo-Jahn-Teller distortion. For Fe^{IV}-imido complexes, our calculations indicate a $d_\delta^2 d_{\delta'}^1 d_\sigma^1$ electronic configuration, which is different from what was proposed in the literature.[68] The degenerate ^3E state under C_{3v} symmetry results in a mild Jahn-Teller distortion and a slightly bent (173°) imido linkage on relaxing the symmetry constraint.

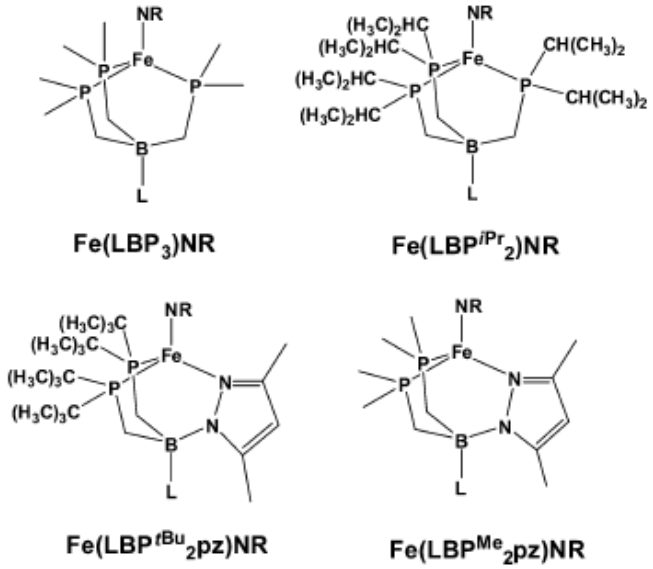

Figure 24. Different ligands considered in this study, depicted as their Fe = NR complexes. R = Me or Ad, L = Me or Ph.

For the Fe^{III}-imido complexes investigated, the excess electronic spin is almost entirely on the iron. Though appearing to be a pure d_{z^2}, the SOMO is also a mix with the N_{Im} p_σ-orbital in an antibonding manner. The spin on the imido nitrogen is cancelled by the spatial offset between the α- and β-spin from the Fe(d_π)-N(p_π) bonding orbitals. The SOMO also has a significant Fe (d_{z^2}) contribution, causing the top lobe to shrink and the bottom lobe to swell (see Figure 25). This provides a possible explanation of the stability of the d_{z^2}-based MO relative to the d_π-based MOs. In essence, the absence of equatorial ligands and of a ligand distal to the imido ligands plays a key role in stabilizing the d_{z^2} orbital as well as the complexes as a whole.

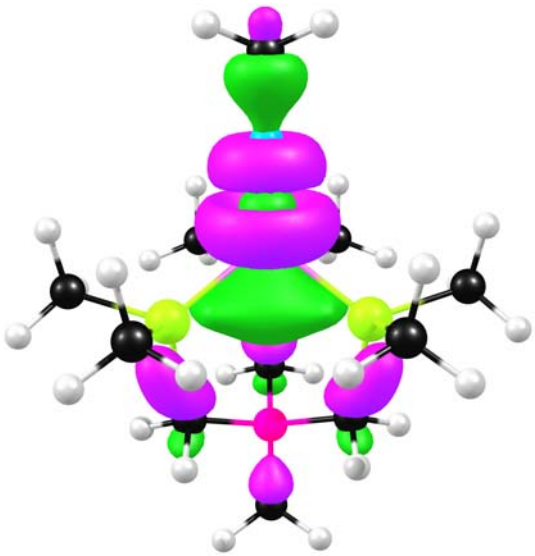

Figure 25. The iron-imido complex SOMO (50% Fe d, 12% Fe p, 9% N). Notice the swollen bottom and the shrunken top.

5-coordinate First-row Transition Metal Terminal Imides

All reported 5 coordinate first-row transition metal terminal imido complexes display SQP coordination geometry, and the first terminal Mn^{V}-imido complex was only recently reported.[78] This corrole Mn-imido complex displayed a square pyramidal coordination geometry with the metal ion 0.5 Å above the average N_4 plane, a Mn-N_{Im} distance of 1.613 Å and a Mn-N-R bond angle of 170.4°. Later reported corrolazine-, the triaza-substituted corrole analogue, Mn^{V}-imido complexes[79] displayed essentially the same geometrical key values, Mn-N_{Im} distances of approximately 1.60 Å and Mn-N-R bond angles of 176.9° and 179.7º. Both the corrole- and the corrolazine Mn^{V} complexes were assigned to be diamagnetic d^2 complexes by spectroscopic methods.[78, 79] As discussed for the four-coordinate imido TMCs, the geometrical key values displayed by these complexes are well within the Mn≡NR bond formalism.[79]

The only possible exception to this is a TBP coordinated possible d^4 intermediate state in the synthesis of iron amido complexes reported by Borovik and coworkers.[80]

The Electronic Structure of TBP Fe^{III}/Mn^{III} Oxo- and Imido Complexes (Paper 3)

In paper 3 we report the electronic and geometrical structure of a class of TBP $metal^{III}$ chalcogenido complexes. The molecules studied are the full experimental triureidoamine ligand complexes reported by Borovik and his group[81, 82] and two simplified models of this (see Figure 26), where the central metal is either iron or manganese. The purpose of this work was to map the electronic structure of this class of 5-coordinated complexes in order to compare with the class of pseudotetrahedral transition metal imido complexes reported by Peters and his group[3] to understand the bonding arrangements of transition metal imido and oxo-complexes.

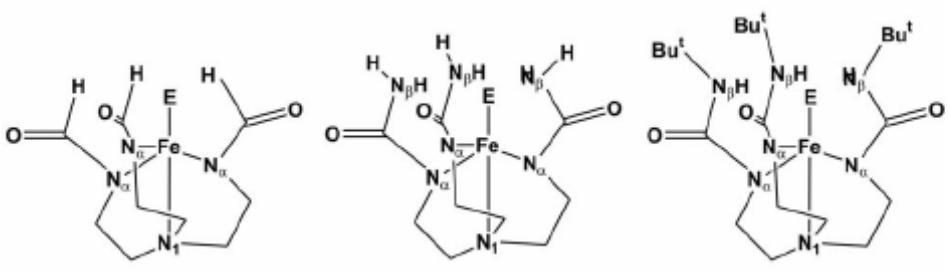

Figure 26. A schematic diagram of the three triureidoamine like ligands systems, L_1, L_2 and L_3, we have used in our computational modeling.

For ligand L_1, the $Fe^{III}O$ distance of 1.75 Å indicates a low bond order, as suggested by Borovik and coworkers.[81, 82] Hydrogen bonding interactions in L_2 and L_3 stretch this distance to about 1.80 Å, which is in good agreement with experiment.[83] This is also seen for the $Fe^{III}S$ and $Fe^{III}Se$ complexes. The $Fe^{III}O$ distance of 1.96 Å in $[Fe^{III}(L_3)(OH)]$ is significantly longer than that in $[Fe^{III}(L_3)(O)]_2$, as expected.[81] Overall the optimized Fe/Mn–E distances agree well with experiment.[81, 82, 84] However, for the Fe–N bonds trans to the Fe^{III}–E unit, our calculations overestimate the bond lengths relative to experiment, in certain cases >0.1Å.

Both the optimized and experimentally observed geometry of $[Fe^{III}(L_3)(O)]^{2-}$ exhibit nearly perfect C_3 symmetry.[82] Thus, the $Fe^{III}O$ oxygen acts as a triple hydrogen bond acceptor in an almost symmetrical manner. In contrast to this, for $[Fe^{III}(L_3)(E)]^2$ for S and Se the lowest lowest-energy optimized geometries deviates significantly from C_3 symmetry.[84]

For the simplest species $[Fe^{III}(L_1)(O)]^2$, the Fe and O are sharing approximately 94% of the overall spin (spin populations of 3.9 and 0.8, respectively). For the L_2 and L_3 complexes, the oxygen spin is smaller, and the iron ion and equatorial nitrogens must therefore compensate by carrying larger parts of the overall spin. An observable trend in the spin density profile is, when going from Mn to Fe, the spin population on the oxygen in the Mn complexes are dramatically lower than those in analogous Fe species, about 1/3 and 1/10 for the $M^{III}(L_3)(O)^{2-}$ and the $M^{III}(L_3)(OH)$, respectively.

The orbital splitting diagram for TBP complexes explains easily the high-spin character of the d^4 TBP complexes ($[Mn(L_3)(O)]^{2-}$), but for d^5 analogues the situation is slightly more subtle. Simple CFT arguments here suggest either S = 5/2 or 3/2 but not 1/2. All the Borovik type complexes are high-spin and this has more to do with their TBP geometries than with the ligand field strengths of the L_3 ligand. For the imido Borovik complexes a wide range of functionals (from post-SCF calculations) predicts the high-spin Fe^{III} and Fe^{IV} cases (S = 5/2 and S = 2) as the ground states. There is a notable difference in bond angle for the Fe-N-C between the Fe^{IV} and the Fe^{III}, the latter being more linear and having a more axially symmetric spin density profile.

For all the functionals used in this study, the $Fe^{III}(L_3)$-oxo and imido complexes were indicated as S = 5/2. For $[Fe^{III}(L_3)(O)]^{2-}$ the 5/2 state was preferred by between 0.2 - 0.6 eV over the S = 3/2 state and by 0.6 - 1.3 eV over the S = 1/2 state. The high-spin state was somewhat less preferred for the Fe^{IV} complexes. The calculations reproduce the experimentally observed high-spin states of these compounds; an analysis based on results from calculations with different functionals suggests that the high-spin nature of these species follows largely from their TBP geometry. Iron d_π – oxo p_π interactions invariably result in a substantial spin density on the oxygen, which in turn may be significantly tuned by hydrogen bonding interactions. The oxygen spin densities are smaller in analogous manganese-oxo species, indicating that manganese is less adept at π-bonding than iron.

More on the side of the scope of this thesis, but still of some interest: Using total bonding energy as taken from the optimized geometry output, we evaluated the H-bond protection of the $Fe^{III}O$ unit in the $Fe^{III}(L_3)(O)^{2-}$ complex. Computing the adiabatic O-protonation affinities

of $[Fe^{III}(L_1)(O)]^{2-}$ and $[Fe^{III}(L_3)(O)]^{2-}$ give us a number of 24.5 kcal/mol, which is a rather large value. Being gas phase numbers, and therefore less of relevance, they still indicate that the hydrogen bonding interactions may play a major role in stabilizing $[Fe^{III}(L_3)(O)]^{2-}$ toward proton-coupled decomposition.

With their TBP geometry, having two ligands on the z-axis, the hybridization of the metal d_{z^2} based MO, as discussed for the pseudotetradral geometries, is not possible. As expected, we see no occupation of this orbital for the Borovik type TBP complexes.

5 CONCLUSIONS

In this thesis, computational methods have been used to investigate the electronic and geometric structures of certain classes of transition metal nitrosyl and imido complexes, with emphasis on 4- and 5-coordinate geometries.

In Paper 1, we showed, among other things, that the presence of a sixth ligand (ImH) (for (Por)Fe(NO)(ImH)) pushes much of the spin density away from the Fe onto the NO. The antibonding metal d_{z^2} - ImH interaction present in the SOMO gives a rather long Fe-N_{ImH} bond. The observed cooperative bending and tilting of the Fe-N_{NO} vector tilted relative to the porphyrin plane normal, is explained by metal d_π-NO π^* and d_σ-NO π^* orbital interactions. These findings are not novel but they serve as a useful reference for understanding the less well-known electronic structures of related nonheme low-coordinate complexes.

In Paper 2, we identified a subtle difference in the nature of the SOMO between SQP and the TBP_{eq} $\{FeNO\}^7$ complexes; for the SQP case the SOMO is primarily Fe d_{z^2}-based, which favors σ-bonding interactions with an NO π^* orbital, giving a bent FeNO unit. In the TBP_{eq} case, the SOMO is best described as Fe $d_{x^2-y^2}$ based, which stretches out less toward the NO and is thus less suitable for σ-bonding with NO π^* orbital, causing π bonding to dominate and leading to an essentially linear FeNO unit. For a sterically unhindered model the SQP and TBP_{eq} stereochemistries are nearly equienergetic, with the former very slightly lower in energy. Steric constraints such as those operating for Fe(5,5-TC)(NO) can reverse this stereochemical preference.

In Paper 4, we assigned a $d_\delta^2 d_{\delta'}^2 d_\sigma^1$ electronic configuration to a low-spin Fe^{III}-imido and a $d_\delta^2 d_{\delta'}^1 d_\sigma^1$ electronic configuration to a Fe^{IV}-imido complex with a tripodal phosphine supporting ligand. The Fe^{III}-imido complex SOMO is essentially an antibonding combination of the metal d_σ orbital and the N_{Im} p_σ orbital. However, a significant amount of metal p_z character also mixes in, causing the bottom lobe of the d orbital to swell at the expense of the

top one. This unique feature reduces the antibonding character of these complexes and indeed is responsible for the very existence and stability of these compounds.

In Paper 3 we assign the high-spin states of iron-chalcogenido complexes to their TBP_{ax} geometries. For the investigated Fe^{III} and Fe^{IV} imido complexes, high-spin S = 5/2 and S = 2 states are predicted as ground states for a wide variety of functionals. In contrast to the pseudotetrahedral complexes reported in Pper 1, the metal d_{xy} and $d_{x^2-y^2}$ orbitals in the TBP complexes do interact strongly with the basal ligand orbitals and are not significantly stabilized relative to the other d orbitals causing the ligand field splitting to be different in the two classes of complexes. With two ligands on the z axis, the d_{z^2} orbital enjoys no special stability, as in the tetrahedral case, and it is perhaps not surprising that no imido complexes have yet been reported for the ligand in question.

The presented studies reveal striking similarities of the electronic structure for the low-coordinate transition metal imido- and nitrosyl complexes relative to each other. The distinction of bent versus linear NO units is attributed to the ranking of the d_{z^2} and $d_{xz/yz}$ parentage MOs relative to each other. Without a ligand trans to the NO group, the antibonding metal d_{z^2} - NO σ orbital interaction is lessened by mixing in metal p_z, causing the MO to shrink away from the NO ligand. This exact same orbital interaction appears to be the explanation of the existence of middle to late first-row transition metal imido complexes, and is not seen for complexes with axial ligands trans to the imido or nitrosyl unit.

REFERENCES

[1] Lippard, S. J.; Berg, J. M. *Principles of Bioinorganic Chemistry*, **1994**, University Science Books, Mill Valley.

[2] Walker, F. A. *J. Inorg. Biochem*. **2005**, *99*, 216.

[3] Mehn, M. P; Peters, J.C. *J. Inorg. Biochem*. **2006**, *100*, 634.

[4] Enemark, J. H.; Feltham, R. D. *Proc. Nat. Acad. Sci. USA*, **1972**, *69*, 3534.

[5] Ghosh, A. *J. Biol. Inorg. Chem*. **2006**, *11*, 712.

[6] Levine, I. N. *Quantum Chemistry*, 4th ed. **1991,** Prentice-Hall Inc, New Jersey.

[7] Cramer, C. J. *Essentials of Computational Chemistry*, **2002**, John Wiley & Sons Ltd, Chichester

[8] Jensen, F. *Introduction to Computational Chemistry*, **1999**, John Wiley & Sons Ltd, Chichester.

[9] Szabo, A.; Ostlund, N. S. *Modern Quantum Chemistry*, **1996**, Dover Publications Inc., Mineola.

[10] Ghosh, A; Taylor, P. R. *Curr. Opin. Chem. Biol.* **2003**, *91*, 113.

[11] Cohen, A. J; Mori-Sánchez, P.; Yang, W. *Science*, **2008**, *321*, 792.

[12] Atkins, P.; Friedman, R. *Molecular Quantum Mechanics,* 4th ed., **2005**, Oxford University Press Inc., New York.

[13] Koch, W; Holthausen, M. C. *A Chemist's Guide to Density Functional Theory* 2nd ed. **2000**, Wiley-VCH Verlag GmbH, Weinheim

[14] Hohenberg, P; Kohn, W. *Phys. Rev*. **1964**, *136*, B864.

[15] Siegbahn, P. E. M.; Blomberg, M. R. A. *Chem. Rev.* **2000**, *100*, 421

[16] Ghosh, A.; Steene, E. *J. Biol. Inorg. Chem.* **2001**, *6*, 739.

[17] Ghosh, A; Persson, B. J.; Taylor, P. R. *J. Biol. Inorg. Chem*. **2003**, *8*, 507.

[18] Ghosh, A.; Gonzalez, E.; Tangen, E.; Roos, B. O. *Journal of Physical Chemistry A*, **2008**, ASAP Article.

[19] Neese, F. *J. Biol. Inorg. Chem.* **2006**, *11*, 702.

[20] Siegbahn, P. E. M. *J. Biol. Inorg. Chem.* **2006**, *11*, 695.

[21] Boese, A. D.; Martin, J. M. L. *J. Chem. Phys.* **2003**, *119*, 3005.

[22] Ghosh, A.; Taylor, P. R. *J. Chem. Theory Comput.* **2005**, *1*, 597.

[23] Baerends, E. J.; Gritsenko, O. V. *J. Phys. Chem. A*, **1997**, *101*, 5383.

[24] Chong, D. P.; Gritsenko, O. V.; Baerends, E. J. *J. Chem. Phys.* **2002**, *116*, 1760.

[25] Bartlett, R. J.; Lotrich, V. F.; Schweigert, I. V. *J. Phys. Chem.* **2005**, *123*, 062205.

[26] (a) te Velde, G.; Bickelhaupt, F.M.; van Gisbergen, S.J.A.; Fonseca Guerra, C.; Baerends, E.J.; Snijders, J.G.; Ziegler, T. *J. Comput. Chem.* **2001**, *22*, 931, (b) Fonseca Guerra, C.; Snijders, J.G.; te Velde, G.; Baerends, E.J. *Theor. Chem. Acc.* **1998**, *99*, 391 (c) ADF2004.01, SCM, Theoretical Chemistry, Vrije Universiteit, Amsterdam, The Netherlands, http://www.scm.com.

[27] http://www.chemcraftprog.com, compliments to mr. Grigoriy A. Zhurko.

[28] Perdew, J. P.; Chevary, J. A.; Vosko, S. H.; Jackson, K. A.; Pederson, M. R.; Singh, D. J.; Fiolhais, C. *Phys. Rev. B* **1991**, *46*, 6671.

[29] Handy, N.C. and A.J. Cohen, *Molecular Physics*, **2001**. *99*, 403.

[30] Lee, C.; Yang, W.; Parr, R.G., *Phys. Rev. B* **1988**, *37*, 785.

[31] The ADF reference list: http://www.scm.com/Doc/Doc2007.01/ADF/ADFUsersGuide/page365.html

[32] Rayner-Canham, G.; Overton, T. *Descriptive Inorganic Chemistry,* 3rd ed., **2003**, W. H. Freeman and Company, New York.

[33] Sharpe, A. G. *Inorganic Chemistry*, **1992**, Longman Scientific & Technical, Harlow.

[34] Cotton, F. A.; Wilkinson, G.; Murillo, C. A.; Bochmann, M. *Advanced Inorganic Chemistry*, 6th ed., **2004**, John Wiley & Sons Pte. Ltd, Singapore.

[35] Owen, S. M.; Brooker, A..T. *A Guide to Modern Inorganic Chemistry*, **1991**, Longman Scientific & Technical, Harlow.

[36] Schriver, D. F.; Atkins, P. W.; Langford, C. H. *Inorganic Chemistry,* 2nd ed. **1994**, Oxford University Press, Oxford.

[37] McCleverty, J. A. *Chem. Rev*. **2004**, *104*, 403.

[38] Tangen, E. Unpublished results.

[39] Enemark, J. H.; Feltham, R. D. *Coord. Chem. Rev.* **1974**, *13*, 339.

[40] Li, H.; Igarashi, J.; Jamal, J.; Yang, W.; Poulos, T. L. *J. Biol. Inorg. Chem*. **2006**, *11*, 753.

[41] Fenske, R. F.; DeKock, R. L. *Inorg. Chem.* **1972**, *11*, 437

[42] Enemark, J. H.; Feltham, R. D. *J. Am. Chem. Soc.* **1974**, *96*, 5002

[43] Hoffmann, R.; Chen, M. M. L.; Elian, M.; Rossi, A. R.; Mingos, D. M. P. *Inorg. Chem.* **1974**, *13*, 2666.

[44] Scheidt, W. R.; Ellison, M. K. *Acc. Chem. Res.* **1999**, *32*, 350.

[45] Ellison, M. K.; Scheidt, W. R. *J. Am. Chem. Soc.* **1997**, *119*, 7404.

[46] Scheidt, W. R.; Duval, H. F.; Neal, T. J.; Ellison, M. K. *J. Am. Chem. Soc.* **2000**, *122*, 4651

[47] Ghosh, A.; Wondimagegn, T. *J. Am. Chem. Soc,* **2000**, *122*, 8101

[48] Wyllie, G. R. A.; Schulz, C. E.; Scheidt, W. R. *Inorg. Chem.* **2003**, *42*, 5722

[49] Xu, C.; Spiro, T. G. *J. Biol. Inorg. Chem*. **2008**, *13*, 613.

[50] Franz, K.J.; Lippard, S. J. *J. Am. Chem. Soc.* **1998**, *120*, 9034

[51] Conradie, J.; Quarless, D. A.; Hsu, H.-F.; Harrop, T. C.; Lippard, S. J.; Koch, S. A.; Ghosh, A. *J. Am. Chem. Soc.* **2007**, *129*, 10446.

[52] Franz, K.J.; Lippard, S. J. *J. Am. Chem. Soc.* **1998**, *121*, 10504.

[53] Conradie, J.; Ghosh, A. *J. Inorg. Biochem.* **2006**, 2069.

[54] Patra, A. K.; Rose, M. J.; Olmstead, M. M.; Mascharak, P. K. *J. Am. Chem. Soc*, **2004**, *126*, 4780.

[55] Walsh, A. D. *J. Chem. Soc.* **1953**, 2266.

[56] Enemark, J. H.; Feltham, R. D. *J. Am. Chem. Soc.* **1974**, *96*, 5004.

[57] Franz, K.; Doerrer, L. H.; Spingler, B.; Lippard, S. J. *Inorg. Chem.* **2001**. *40*, 3774.

[58] Harrop, T. C.; Song, D.; Lippard, S. J. *J. Am. Chem. Soc*, **2006**, *128*, 3528.

[59] Conradie, J.; Ghosh, A. *J. Inorg. Biochem.* **2006**, *100*, 2069.

[60] From Rob Torakis Organometallic Hypertextbook: http://www.ilpi.com/organomet/imido.html, downloaded 26.07.08.

[61] Nugent, W. A.; Haymore, B. L. *Coord. Chem. Rev.* **1980,** *31*, 123.

[62] Eikey, R. A.; Abu-Omar, M. M. *Coord. Chem. Rev.* **2003**, *243*, 83 and references therein.

[63] Dai, X.; Kapoor, P.; Warren, T. H. *J. Am. Chem. Soc.* **2004**, *126*, 4798.

[64] Kogut, E.; Wiencko, H. L.; Zhang, L.; Cordeau, D. E.; Warren, T. H. *J. Am. Chem. Soc*. **2005**, *127*, 11248.

[65] Eckert, N. A.; Vaddadi, S.; Stoian, S.; Lachicotte, R. J.; Cundari, T. R.; Holland, P. L. *Angew. Chem. Int. Ed.* **2006**, *45*, 6868.

[66] Conradie, J.; Ghosh, A. *J. Chem. Theory. Comput.* **2007**, *3*, 689.

[67] Verma, A. K.; Nazif, T. N.; Achim, C.; Lee, S. C. *J. Am. Chem. Soc.* **2000**, *122*, 11013.

[68] Thomas, C. M.; Mankad, N. P.; Peters, J. C. *J. Am. Chem. Soc.* **2006**, *128*, 4956.

[69] Lu, C.; Peters, J. C. *Inorg. Chem.* **2006**, *45*, 8597.

[70] Brown, S. D.; Betley, T. A.; Peters, J. C. *J. Am. Chem. Soc.* **2003**, *125*, 322.

[71] Brown, S. D.; Peters, J. C. *J. Am. Chem. Soc.* **2005**, *127*, 1913.

[72] Mehn, M. P.; Brown, S. D.; Jenkins, D. M.; Peters, J. C.; Que, L. Jr. *Inorg. Chem.* **2006**, *45*, 7417.

[73] Jenkins, D. M.; Betley, T. A.; Peters, J. C.; *J. Am. Chem. Soc.* **2002**, *124*, 11238.

[74] Shay, D. T.; Yap, G. P. A.; Zakharov, L. N.; Rheingold, A. L.; Theopold, K. H. *Angew. Chem. Int. Ed.* **2005**, *44*, 1508, corrigendum *Angew. Chem. Int. Ed*. **2006**, *45*,7870

[75] Hu, X.; Meyer, K. *J. Am. Chem. Soc*. **2004**, *126*, 16322.

[76] Stark, J. G; Wallace, H. G. *Chemistry Data Book,* 2nd ed. in SI, **1982**, John Murray Ltd, London.

[77] Wasboten, I. H.; Ghosh, A. *Inorg. Chem.* **2007**, *46*, 7890.

[78] Eikey, R. A.; Khan, S. I.; Abu-Omar, M. M. *Angew. Chem. Int. Ed.* **2002**, *41*, 3591.

[79] Goldberg, D. P. *Acc. Chem. Res.* **2007**, *40*, 626.

[80] Lucas, R. L.; Powell, D. R.; Borovik, A. S. *J. Am. Chem. Soc.* **2005**, *127*, 11596.

[81] MacBeth, C. E.; Gupta, R.; Mitchell.-Koch, K. R.; Young Jr., V. G.; Lushington, G. H.; Thompson, W. H.; Hendrich, M. P.; Borovik, A. S. *J. Am. Chem. Soc.* **2004**, *126*, 2556.

[82] Borovik, A. S. *Acc. Chem. Res*. **2005**, *38*, 54.

[83] MacBeth, C. E.; Golombek, A. P.; Young Jr., V. G.; Yang, C.; Kuczera, K.; Hendrich, M. P.; Borovik, A. S. *Science* **2000**, *289*, 938.

[84] Larsen, P. L.; Gupta, R.; Powell, D. R.; Borovik, A. S. *J. Am. Chem. Soc.* **2004**, *126*, 6522.

Paper 1

Toward Modeling H-NOX Domains: A DFT Study of Heme-NO Complexes as Hydrogen Bond Acceptors.

Tangen, E.; Svadberg, A.; Ghosh, A.

Inorganic Chemistry **2005**, *44*, 7802-7805.

(*NB*: Active link)

Paper 2

The Challenge of Being Straight: Explaining the Linearity of a Low-Spin $\{FeNO\}^7$ Unit in a Tropocoronand Complex

Tangen, E.; Conradie, J.; Ghosh, A.

Inorganic Chemistry **2005**, *44*, 8699-8706.

(*NB*: Active link)

Paper 3

Trigonal bipyramidal iron(III) and manganese(III) oxo, sulfido, and selenido complexes. An electronic-structural overview.

Conradie, J.; Tangen, E.; Ghosh, A.

Journal of Inorganic Biochemistry **2006**, *100*, 707-715.

(*NB*: Active link)

Paper 4

Bonding in Low-Coordinate Environments: Electronic Structure of Pseudotetrahedral Iron-Imido Complexes.

Tangen, E.; Conradie, J.; Ghosh, A.

J. Chem. Theory Comput. **2007**, *3*, 448-457.

(NB: Active link)

ISBN 978-82-92461-95-2